 doi:10.20944/preprints202208.0159.v1

Article

Phosphatidylethanolamine *N*-methyltransferase knockout modulates metabolic changes in aging mice

Qishun Zhou [1†], Fangrong Zhang [1,2†], Jakob Kerbl-Knapp [1], Melanie Korbelius [3], Katharina Barbara Kuentzel [3], Nemanja Vujić [3], Alena Akhmetshina [3], Gerd Hörl [4], Margret Paar [4], Ernst Steyrer [2], Dagmar Kratky [2,5], and Tobias Madl [1,5,*]

[1] Gottfried Schatz Research Center for Cell Signaling, Metabolism and Aging, Molecular Biology and Biochemistry, Research Unit Integrative Structural Biology, Medical University of Graz, 8010 Graz, Austria; qishun.zhou@medunigraz.at (Q.Z.); jakob.kerbl-knapp@stud.uni-heidelberg.de (J.K.-K.); tobias.madl@medunigraz.at (T.M.)

[2] Key Laboratory of Gastrointestinal Cancer (Fujian Medical University), Ministry of Education, Fuzhou, China; fangrongzhang@fjmu.edu.cn (F.Z.)

[3] Gottfried Schatz Research Center for Cell Signaling, Metabolism and Aging, Molecular Biology and Biochemistry, Medical University of Graz, 8010 Graz, Austria; m.korbelius@medunigraz.at (M.K.); katharina.kuentzel@medunigraz.at (K.B.K.); nemanja.vujic@medunigraz.at (N.V.); alena.akhmetshina@medunigraz.at (A.A.); ernst.steyrer@medunigraz.at (E.S.); dagmar.kratky@medunigraz.at (D.K.)

[4] Otto-Loewi Research Center, Division of Medicinal Chemistry, Medical University of Graz, 8010 Graz, Austria; gerd.hoerl@medunigraz.at (G.H.); margret.paar@medunigraz.at (M.P.)

[5] BioTechMed-Graz, 8010 Graz, Austria

* Correspondence: tobias.madl@medunigraz.at; Tel.: +43-316-385-71972; Fax: +43-316-385-79615

† Equal contribution

Abstract: Phospholipid metabolism, including phosphatidylcholine (PC) biosynthesis, is crucial for various biological functions and is associated to longevity. Phosphatidylethanolamine *N*-methyltransferase (PEMT) is a protein that catalyzes the biosynthesis of PC, the levels of which change in various organs such as brain and kidney during aging. However, the role of PEMT for systemic PC supply is not fully understood. To address how PEMT affects aging-associated energy metabolism in tissues responsible for nutrient absorption, lipid storage and energy consumption, we employed NMR-based metabolomics to study liver, plasma, intestine (duodenum, jejunum, ileum), brown/white adipose tissues (BAT, WAT), and skeletal muscle of young (9–10 weeks) and old (96–104 weeks) wild-type (WT) and PEMT knockout (KO) mice. We found that the effect of PEMT-knockout was tissue-specific and age-dependent. Deficiency of PEMT affected the metabolome of all tissues examined, among which the metabolome of BAT from both young and aged KO mice was dramatically changed in comparison to WT mice, whereas the metabolome of jejunum was only slightly affected. As for aging, the absence of PEMT increased the divergence of metabolome during aging of liver, WAT, duodenum and ileum and decreased the impact on skeletal muscle. Overall, our results suggest that PEMT plays a previously unexplored critical role in both aging and energy metabolism.

Keywords: metabolomics; NMR; PEMT; knockout; aging; mice; liver; intestine; white/brown adipose tissue

1. Introduction

Aging affects the physiology of living organisms, causes a multitude of defects in biological functions, and is induced by orchestrated alterations in various metabolic path-

 doi:10.20944/preprints202208.0159.v1

ways [1-3]. Systematic studies, particularly during the past decades, investigated the biological features of aging at the cellular, transcriptomic, proteomic, metabolomic, and molecular levels [4-9] and have linked a remarkable number of biological mechanisms to aging. Dysregulated lipid metabolism contributes to aging via various complex mechanisms [10-12]. An emerging body of data indicates that biosynthesis of phospholipids (PLs), triglycerides, fatty acids, and sphingolipids plays a key role in lifespan regulation [13-15]. Notably, PLs are the major components of membranes in eukaryotic cells [16,17], and their association to aging has been demonstrated recently [18]. Phosphatidylcholine (PC) and phosphatidylethanolamine (PE) are the two most abundant PLs in mammalian cells and are important building blocks for more complex PLs [14,19,20]. They also play critical roles in processes such as biosynthesis of biological membranes, lipid transport via lipoproteins, lipid droplet formation [21], regulation of mitochondrial function, cell proliferation/apoptosis, insulin signaling, and whole-body energy homeostasis [19,22,23].

The biosynthesis of PC from PE in mammals is catalyzed by phosphatidylethanolamine *N*-methyltransferase (PEMT) via 3 sequential steps of PE methylation by transferring the methyl group from S-adenosylmethionine to the corresponding substrates, i.e., PE, phosphatidylmonomethylethanolamine, and phosphatidyldimethylethanolamine [24-26]. This process mediates about 30% of liver PC biosynthesis and is one of three PC biosynthesis pathways in mammalian cells [27,28]. PEMT1 and PEMT2 are the two isoforms of PEMT, with PEMT1 localized in the endoplasmic reticulum (ER) and PEMT2 in the mitochondria-associated membranes (MAM) [29,30]. They are encoded by the same gene and perform the same enzymatic activities [31]. The other two biosynthetic pathways of PC are the cytidine-5′-diphosphocholine (CDP-choline) pathway, which adds CDP-choline to diacylglyceride, and the Lands cycle, which adds a fatty acid to lysophosphatidylcholine [27,32]. The PEMT pathway is therefore the only pathway to synthesize PC independent of dietary choline or its derivatives, and disruption of the PEMT pathway in combination with a choline-deficient diet is lethal to knockout mice. [30]. PEMT has a prominent role for the secretion of very low-density lipoproteins (VLDL) by the liver [19,33,34], and regulates the formation of lipid droplets (LD) by adipocytes [21]. Furthermore, the PEMT and CDP-choline pathways have been found to yield PCs with fatty acids of different lengths and degrees of unsaturation in yeast cells and rat hepatocytes, which may underline the importance of the respective pathways [35,36]. Additionally, the extent to which PC concentration changes in the liver of PEMT KO mice remains unclear. Controversial results have been found regarding the hepatic PC concentration under PEMT deficiency [31,37], and a recent study indicated lower mitochondrial PC level in the KO liver [38]. Taking together the subcellular enrichment of PEMT on ER and MAM [21,30], both total and subcellular PC levels in the KO liver remain elusive. PEMT deficiency leads to various biological changes, including increased hepatic steatosis [39], attenuated ER stress in diabetic nephropathy [40], resistance to diet-induced obesity, and protection against insulin resistance in mice [41-43]. These observations suggest a unique role for PEMT in lipid metabolism.

It is unclear whether methylation of PE by PEMT regulates the progression of aging because the levels of both substrate and product, i.e. PE and PC, are found to either increase or decrease in various aged tissues from human, mouse, or nematodes [18]. Interestingly, dietary supplementation of both PE and PC has been found to contribute to lifespan extension in *C. elegans* through the same mechanism that reduces insulin/IGF-1-like signaling and promotes DAF-16 activity [44-46]. Several unsaturated PCs play a protective role against neurodegenerative diseases in humans [18]. A decrease in PE levels with aging has been observed in *C. elegans* and mice [47,48], whereas an increase in PE levels prolonged lifespan in yeast and flies and increased the replicative viability of mam-

 doi:10.20944/preprints202208.0159.v1

malian cells [49]. While PEMT is of particular importance for lipid metabolism and membrane biosynthesis, a systematic investigation of the molecular basis of its function is required to elucidate additional functions of PEMT beyond its function in PC synthesis.

Mouse models are well suited to study age-related metabolic changes due to their analogy to human metabolism [50-52]. Here, we investigated the role of PEMT in lipid metabolism and energy homeostasis in young (9-10 weeks) and old (96-104 weeks) wild-type (WT) and PEMT knockout (KO) mice. Using untargeted NMR-based metabolomics, we assessed metabolic alterations caused by PEMT deficiency in liver, intestine (duodenum, jejunum, and ileum), plasma, brown and white adipose tissues (BAT, WAT), and skeletal muscle. Liver is the tissue with the by far highest expression level of PEMT [53]. We expected to observe the direct consequence of PEMT KO on the metabolism of the aforementioned tissues, especially the liver, as well as homeostasis of PC in corresponding tissues to compensate for the lack of PEMT-derived PC. Furthermore, we aimed to identify the indirectly linked metabolic alterations in these tissues in response to PEMT deficiency, including potential secondary or remote effects.

We addressed the identification of changes in the metabolome through pairwise comparison of WT and KO tissues, or young and aged tissues, respectively. Most KO tissues displayed moderate changes in their metabolome. Notably, the metabolome of BAT from both young and old mice, as well as liver and ileum from young mice, were dramatically affected by the loss of PEMT. Associated with this, we identified a large number of significantly altered metabolites in each of these tissues. The impact of PEMT deficiency on the metabolome of liver and BAT appeared to be largely age-independent, suggesting that these are the core tissues driving the metabolic changes in KO mice. As for their aging profiles, we identified metabolites as aging biomarkers that were either increased or decreased in the KO tissues. All KO tissues had altered sets of aging biomarkers compared with their WT counterparts. PEMT-deficient skeletal muscle displayed fewer aging biomarkers than WT skeletal muscle. The aging profiles of plasma and BAT remained mostly PEMT independent. Notably, the aging metabolome of liver, WAT, duodenum, and ileum from KO tissues were associated with more aging biomarkers than the WT tissues. This suggested that their metabolic adaptations to the lack of PEMT are highly affected by aging, resulting in a strong add-on effect. Jejunum remained metabolically unchanged both during aging and PEMT KO, demonstrating its metabolic stability. These results indicate that PEMT plays a critical role in energy metabolism by regulating the function of most associated tissues and their functional changes during aging.

2. Materials and Methods

2.1. Animals

Mice globally lacking PEMT were generated in the laboratory of Dennis E. Vance on a mixed genetic background (129/J and C57BL/6J). Young (9-10 weeks of age) and old (96-104 weeks of age) female mice were housed in a temperature-controlled environment with *ad libitum* access to food (standard chow diet; 11.9% caloric intake from fat; Altromin, Lage, Germany) and water in a regular light-dark cycle (12 h/ 12 h). Organs were collected after overnight fasting. All experiments were performed in accordance with the European Directive 2010/63/EU. Metabolomic studies of several tissues of aged WT mice have been published previously [52].

2.2. Pretreatment of NMR Samples

From each tissue, 30 - 50 mg were isolated, snap-frozen in liquid nitrogen, and stored at −80 °C until metabolite extraction. To isolate metabolites, 400 µL ice-cold methanol and 200 µL MilliQ H_2O were added to each tissue sample, while 400 µL ice-cold methanol was added to 200 µL plasma sample. Tissue homogenization was performed using the Precellys 24 tissue homogenizer (Bertin Technologies, Montigny-le-Bretonneux, France) in 2 mL

 doi:10.20944/preprints202208.0159.v1

tubes with O-ring caps and Precellys beads (1.4 mm zirconium oxide beads, Bertin Technologies, Villeurbanne, France). The homogenized tissues were centrifuged at 13,000 rpm for 45 min (4 °C), after which the supernatants were transferred into new 1.5 mL tubes, and lyophilized at <1 Torr, 850 rpm, 25 °C for 10 h in a vacuum-drying chamber (Savant Speedvac SPD210 vacuum concentrator) with an attached cooling trap (Savant RVT450 refrigerated vapor trap) and vacuum pump (VLP120) (all Thermo Scientific, Waltham, MA, USA). The lyophilized samples were subsequently dissolved in 500 µL NMR buffer (0.08 M Na_2HPO_4, 5 mM TSP (3-(trimethylsilyl) propionate-2,2,3,3-d4 sodium salt, 0.04 (w/v)% NaN_3 in D_2O, pH adjusted to 7.4 with 8 M HCl and 5 M NaOH) for NMR analysis. For lipid removal, 50 µL chloroform ($CHCl_3$) was added to the tissue lysates of BAT, WAT, and intestine and centrifuged at 13,000 rpm for 10 min (4 °C). The supernatants were transferred to 5 mm NMR tubes for data collection.

2.3. Data Acquisition and Analysis

Metabolic profiling was conducted at 310 K using a 600 MHz Bruker Avance Neo NMR spectrometer (Bruker Biospin, Rheinstetten, Germany) equipped with a TXI 600S3 probe head. ^{1}H ^{1}D NMR spectra were recorded using Carr–Purcell–Meiboom–Gill (CPMG) pulse sequence with a pre-saturation for water suppression (cpmgpr1d, 512 scans, 73,728 points in F1, 12019.230 Hz spectral width, 1024 transients, recycle delay 4 s) [54,55], and ^{1}H-^{13}C heteronuclear single-quantum correlation (HSQC) spectra were recorded with a recycle delay of 1.0 s, spectral widths of 20.8/83.9 ppm, centered at 3.9/50.0 ppm in ^{1}H/^{13}C, with respectively 2048/ 256 points, and 8 scans per increment. NMR spectral data were processed in Bruker Topspin version 4.0.2 using one-dimensional exponential window multiplication of the FID, Fourier transformation, and phase correction as previously described [56]. TSP was used as the internal standard for chemical-shift referencing (set to 0 ppm), and processed NMR data were imported into Matlab2014b. Signal suppressions were applied to regions close to the ^{1}H chemical shift of water, TSP, and methanol (and $CHCl_3$ for BAT, WAT, and intestines, as well as EDTA for plasma). Due to field homogeneity issues, some samples (mainly BAT and WAT) had to be excluded from the data analysis. Alignment and a probabilistic quotient normalization were performed to the ^{1}H ^{1}D NMR spectra by Matlab2014b to generate normalized spectra and reduced spectra. Metabolite quantification was based on the signal integration of normalized spectra as described previously [52]. Signal integration was used to generate a volcano plot, orthogonal partial least squares discriminant analysis (O-PLS-DA), permutation analysis, sparse partial least squares discriminant analysis (S-PLS-DA), metabolite set enrichment analysis (MSEA, only over representation analysis (ORA) was performed here [57]), and a heat map using MetaboAnalyst 5.0 [58]. Statistical significance was tested by quality assessment statistic Q^2. A univariate statistical analysis was carried out for quantified metabolites using GraphPad Prism 7.04 (GraphPad Software, La Jolla, CA, USA). For plotting the statistical analysis in the supplementary figures, data were shown as mean ± standard deviation (SD). An unpaired two-tailed Student's t-test was used to calculate *p*-values for comparison of variables. Metabolites with $p < 0.05$ are shown in panel B and panel D of supplementary Figure S1-S13. For each tissue, an additional 2D ^{1}H-^{13}C HSQC spectra was recorded to highlight the presented metabolites and to validate the interpretations of 1D ^{1}H spectra either published previously (for WT [52]) or included in Supplementary Figure S16.

3. Results

Comparison of individual metabolites revealed a set of increased and decreased metabolites for each tissue. These characteristic metabolic fingerprints partly diverged from biomarkers of aging and manifested as tissue-specific profiles.

 doi:10.20944/preprints202208.0159.v1

3.1. The liver metabolome strongly responds to the absence of PEMT

The livers of young mice were more sensitive to PEMT deficiency than livers of aged mice (Figure 1A, 1C). In young PEMT KO mice, this was associated with an increase in the concentrations of AMP, histidine, acetic acid, UDP-sugars, inosine, ADP, bile acids, glutamine, propionate, and glutathione, and a decrease in the concentration of mannose, hypoxanthine, choline, phosphorylcholine, phenylalanine, glycine, glycerol, and glucose. Among these metabolites, the concentrations of AMP (5.6-fold), histidine (3.1-fold), and UDP-glucose (2.1-fold) were increased by > 2-fold in KO mice compared to WT mice, whereas the level of mannose was decreased by 2.1-fold. The concentration changes of other metabolites were < 2-fold (Figure 1A, Supplementary Figures S1A, S1B). O-PLS-DA yielded a score of 33.2% for the predictive component (T score [1]) and resulted in a good separation of the two groups, associated with a R^2X of 0.332, a R^2Y of 0.977, and a Q^2 at 0.867, indicating a predictive accuracy of the O-PLS-DA model (Figure 1B). We further performed a permutation test and obtained correlation coefficients R^2Y up to 0.997 ($p < 0.01$) and Q^2 up to 0.915 ($p < 0.01$), which suggested a significant distinction between the two groups (Figure 1E).

In the hepatic metabolome of aged KO mice, we observed an increase in the levels of histidine (8.0-fold), AMP (6.0-fold), inosine (2.3-fold), acetic acid, propionate, and glutathione (< 2-fold when not specified), as well as a decrease in the levels of fumarate (2.3-fold), phosphorylcholine, choline, and UDP-N-acetylglucosamine (Figure 1C, Supplementary Figures S2A, S2B). O-PLS-DA yielded a T1 score of 20.7% for the predictive component (Figure 1D). The permutation test additionally yielded correlation coefficients R^2Y of 0.996 ($p < 0.01$) and Q^2 of 0.946 ($p < 0.01$), indicating that the groups can be discriminated with high accuracy by the O-PLS-DA model.

Graphical representation of the four liver groups (S-PLS-DA) yielded a component 1 of 26.1% and a component 2 of 15.6%. All four groups clustered and separated well from each other (Figure 1G). The PEMT KO livers shared multiple aging-related biomarkers with WT livers, including lactate, niacinamide, fumarate, alanine, inosine and aspartate (Supplementary Figure S14A, S14B and previously published results [59]). To investigate the biological relevance of the metabolic changes, we eventually performed an overrepresentation analysis (ORA), an enrichment analysis of metabolite set enrichment analysis (MSEA) [57], with the aim of highlighting biological pathways associated with altered metabolite levels. In young and aged livers, 23 and 11 metabolic pathways, respectively, were associated with the changes, with the 7 major pathways being galactose metabolism, ammonia recycling, lactose synthesis, glutamate metabolism, purine metabolism, PC biosynthesis, and alanine metabolism in young livers (Figure 1H), as well as aspartate metabolism, PC biosynthesis, pyruvate metabolism, ethanol degradation, phenylalanine and tyrosine metabolism, purine metabolism and PL biosynthesis in aged livers (Figure 1I).

3.2. Aging aggravates the effects of PEMT deficiency in plasma

In the plasma of young mice, PEMT deficiency resulted in a 2.9-fold increase in the uremic metabolite indoxyl sulfate (Figure 2A, Supplementary Figures S3A, S3B) without affecting the abundance of other metabolites. O-PLS-DA yielded a consistent score of 13.4% for the predictive component (T score [1]), in association with a low degree of separation (Figure 2B). The permutation test resulted in a R^2Y of 0.979 ($p = 0.01$) and Q^2 of 0.648 ($p = 0.02$), which indicated a significant difference of the two groups (Figure 2E).

In the plasma of aged KO mice, the volcano plot showed a less than 2-fold increase in the levels of isoleucine, lactate, glucose, alanine, and glycerol, accompanied by decreased levels of citrate, myo-inositol, indoxyl sulfate, isobutyrate, and creatine, among which citrate decreased more than 3-fold and myo-inositol decreased to 2.2-fold (Figure

 doi:10.20944/preprints202208.0159.v1

2C, Supplementary Figures S3C, S3D). The T score of the predictive component of the O-PLS-DA plot was 24.3%, consistent with good predictive accuracy due to the distinct clustering of the two groups (Figure 2D). The permutation test yielded a R^2Y of 0.902 ($p = 0.02$) and Q^2 of 0.731 ($p = 0.01$) (Figure 2F).

Plotting the four plasma groups on the S-PLS-DA plot resulted in a component 1 at 30.8% and a component 2 at 18.2% and yielded a distinct separation of WT young and old, as well as between old WT and KO mice (Figure 2G). The aging profile of WT and PEMT KO plasma has both 13 increased and decreased metabolites, 6 of which overlap, suggesting that PEMT affects the metabolic aging of plasma (Supplementary figure S14C, S14D [52]). ORA showed that metabolites with altered levels in the aged KO plasma were related to 5 metabolic pathways, including galactose metabolism, glucose-alanine cycle, Warburg effect, transfer of acetyl groups into mitochondria, and gluconeogenesis (Figure 2H).

3.3. Aging and PEMT deficiency affect skeletal muscle metabolites in opposite ways

It has been previously shown that PEMT KO mice exhibit increased energy expenditure along with elevated basal oxygen consumption rate in skeletal muscles [60]. In line with this, we observed metabolic changes in the skeletal muscles of both young and aged PEMT KO mice compared to the corresponding WT animals (Figure 3A, 3C). As demonstrated in the volcano plot, young muscle tissues showed around 1.5-fold higher concentrations of acetate and reduced concentrations of inosine, malonate, phenylalanine, valine, and glutamate (Figure 3A, Supplementary Figures S4A, S4B), consistent with the score of the first predictive component at 27.3% on the O-PLS-DA plot (Figure 3B). The separation of the two groups was significant, as demonstrated by a permutation test yielding R^2Y of 0.986 ($p = 0.01$) and Q^2 of 0.825 ($p = 0.01$) (Figure 3E).

Quantification of metabolites in skeletal muscle samples from old mice showed an increase in acetate, glycine, and succinate levels, along with a decrease in inosine, malonate, leucine, lysine, and phenylalanine concentrations (Figure 3C, Supplementary Figures S5A, S5B). For O-PLS-DA, a T1 score at 19.9% was obtained (Figure 3D). The significant separation of the two groups was further emphasized by the permutation test with a correlation coefficient R^2Y of 0.985 ($p < 0.01$) and Q^2 of 0.715 ($p < 0.01$) (Figure 3F).

The S-PLS-DA plot showed a distinct separation of all four groups (Figure 3G), with different components separating samples from young/old and WT/KO mice. In addition, only 3 of 15 biomarkers of aging skeletal muscle were conserved in skeletal muscle of PEMT KO mice (Supplementary Figure S14E, S14F and reference [52]). This suggests that aging of skeletal muscle is regulated by PEMT but is not fully PEMT-dependent. ORA showed that changed metabolites from young skeletal muscle were associated with six pathways: Aspartate metabolism, phenylalanine and tyrosine metabolism, amino sugar metabolism, fatty acid biosynthesis, propanoate metabolism, and valine, leucine and isoleucine degradation (Figure 3H). Metabolites from aged samples were associated with three pathways: Carnitine synthesis, aspartate metabolism, and fatty acid biosynthesis (Figure 3I).

3.4. PEMT deficiency strongly affects the metabolic profile of brown adipose tissue

Among the eight specimen we examined in this study, BAT is one of the most metabolically altered tissues in the absence of PEMT. In the volcano plot representing the metabolites detected in BAT of young mice, we observed an increase in inosinate (> 5-fold), citrate, inosine, methionine, and creatine, as well as a decrease in tryptophan and UDP-sugars (> 8-fold), hypoxanthine, valine, alanine, lactate, histidine, isoleucine, acetate, glutamate, glycerophosphocholine, uridine, leucine, phenylalanine, niacinamide, mannose,

 doi:10.20944/preprints202208.0159.v1

and uracil (Figure 4A, Supplementary Figures S6A, S6B). Discriminant clustering of two groups on the O-PLS-DA resulted in a score of the first predictive component of 46.7%, and the significance of their separation was validated by a permutation study with R^2Y of 0.997 ($p = 0.02$) and Q^2 of 0.970 ($p = 0.02$) (Figure 4B, 4E).

We found a similar distinction when comparing old WT and PEMT KO mice, yielding a concentration increase of inosinate (≈ 15-fold), fumarate, and threonine, accompanied by a decrease in tryptophan (≈ 8-fold), UDP-sugars, and histidine (≈ 4-fold), acetate, formate, glycerophosphocholine, isoleucine, valine, phenylalanine, leucine, 3-hydroxybutyrate, glutamine, tyrosine, ethanolamine, and glutamate (Figure 4C, Supplementary Figures S7A, S7B). 11 of the 22 metabolites which are either increased or decreased in the young KO BAT were found to change in a comparable trend in the aged KO BAT (Supplementary Figure S7C). O -PLS-DA showed a clustering with T1 score at 34.6%, whereas permutation validation yielded a R^2Y of 0.986 ($p < 0.01$) and Q^2 of 0.892 ($p < 0.01$) (Figure 4D, 4F).

Notably, the S-PLS-DA plot showed a clear separation of the four groups, especially between the WT and KO groups. (Figure 4G). In the aging profile, eight of the 14 aging biomarkers found in the WT tissues were also conserved in the KO tissues. These biomarkers are highlighted in the Venn diagram and are labeled on the volcano plot corresponding to the aging of KO BAT (Supplementary Figure S7D, S14G, S14H, [52]). This suggests an essential role of PEMT in BAT metabolism, which is partially aging-independent. We further performed ORA using altered metabolites from young and old BAT. The metabolites identified in young tissues were related to glucose-alanine cycle, glycine and serine metabolism, beta-alanine metabolism, valine, leucine and isoleucine degradation, aspartate metabolism, and alanine metabolism (Figure 4H). The metabolites from aged tissues were related to aspartate metabolism, phenylalanine and tyrosine metabolism, urea cycle, ammonia recycling, valine, leucine and isoleucine degradation, amino sugar metabolism, and purine metabolism (Figure 4I). This finding further demonstrates that PEMT manifests both aging-dependent and -independent effects on BAT metabolism.

3.5 PEMT plays a prominent role in WAT during aging

In contrast to BAT, PEMT deficiency had no strong impact on WAT metabolites (Figure 5A, 5C). In young mice, PEMT KO merely caused a decrease in acetate and glucose by less than 2-fold (Figure 5A, Supplementary Figures S8A, S8B). Separation of the 2 groups in the O-PLS-DA plot displayed a T1 score of 19.1% (Figure 5B), and the significance of clustering was addressed by a permutation test with R^2Y of 0.988 ($p < 0.01$) and Q^2 of 0.859 ($p < 0.01$) (Figure 5E).

As in plasma, most of the metabolic alterations were found in the WAT of old mice with an increase of threonine, serine, and arginine by less than 2-fold, together with a decrease of formic acid by more than 3-fold, and a decrease in glucose, glycerol, lactate, and acetate by more than 2-fold. 3-hydroxybutyrate and citrate were both decreased by less than 2-fold (Figure 5C, Supplementary Figures S8C, S8D). O-PLS-DA resulted in a clustering of the two groups with a T1 score of 39.4% (Figure 5D). The permutation test yielded an R^2Y of 0.993 ($p = 0.02$) and Q^2 of 0.779 ($p < 0.01$) (Figure 5F).

The S-PLS-DA plot showed a distinct separation of all four groups, with the WT and KO groups aging differently (Figure 5G). This was further confirmed by the volcano plot of WAT from PEMT KO mice, which were dramatically different from those of WT mice (Supplementary Figure S15A, S15B, [52]) This suggested an interplay between PEMT and aging in the regulation of WAT metabolism, with the role of PEMT gaining importance during aging. ORA indicated that PEMT KO in the aged WAT affected the Warburg effect,

 doi:10.20944/preprints202208.0159.v1

glycine and serine metabolism, transfer of acetyl groups into mitochondria, aspartate metabolism, gluconeogenesis, fatty acid biosynthesis, and galactose metabolism (Figure 5H).

3.6. Intestinal segments respond differently to PEMT KO.

The duodenum, the first part of the small intestine, showed an insensitive aging profile [52], however, this changed with PEMT deficiency. In tissues of young KO mice, we observed an increase in fumarate and a decrease in formic acid, choline, mannose, ethanolamine, glycine, lysine, lactate, and threonine (Figure 6A, Supplementary Figure S9A, S9B). Among these metabolites, only formic acid was decreased by more than 2-fold. The two groups were clustered on the O-PLS-DA plot with the score of the first predictive component of 31.2% (Figure 6B). In addition, permutation yielded a R^2Y at 0.895 ($p = 0.02$) and Q^2 at 0.681 ($p = 0.01$) (Figure 6E). Tissues of aged KO mice had a different set of altered metabolites, including increased dCTP, UDP-sugars, glucose, and guanosine and decreased uridine, formic acid, histidine, and ethanolamine (Figure 6C, Supplementary Figures S10A, S10B). Only dCTP increased more than 2-fold. O-PLS-DA showed a T1 score of 15.6% (Figure 6D), and permutation resulted in an R^2Y of 0.997 ($p < 0.01$) and Q^2 of 0.892 ($p < 0.01$) (Figure 6F). On the S-PLS-DA plot, the two WT groups were clearly separated from the two KO groups, which was consistent with the volcano plot. Furthermore, the two KO groups were partly separated from each other with greater difference between young and aged PEMT KO mice compared to their WT counterparts (Figure 6G, Supplementary Figure S15C, S15D). Taken together, these results indicate that PEMT changes the metabolism of young and aged duodena in a distinct way, and its deficiency affects the metabolic stability of the duodenum. Enrichment analysis by ORA revealed PEMT-associated pathways in the young duodenum such as the biosynthesis of various PLs, and carnitine synthesis, (Figure 6H), whereas in the aged duodenum, identified metabolites were related to lactose synthesis, methylhistidine metabolism, galactose metabolism, and sphingolipid metabolism (Figure 6I). The overall difference between the two sets of pathways clearly suggests a drastic change in the role of PEMT during duodenal aging.

Like the duodenum, the jejunum was shown in our previous studies as an "unaged" organ whose metabolic profile remained unchanged in old mice [52]. Here, we additionally demonstrated its insensitivity to PEMT deficiency (Figure 7A, 7C). Jejuna from young PEMT KO mice displayed solely an increase in fumarate (2.7-fold) and decreased levels of arginine and alanine by less than 2-fold (Figure 7A, Supplementary Figures S11A, S11B). O-PLS-DA resulted in a clustering of the two groups with a T1 score of 26.4% (Figure 7B), and the permutation rendered R^2Y at 0.991 ($p = 0.04$) and Q^2 at 0.626 ($p = 0.1$), indicating an insignificant separation (Figure 7E). Uridine and inosine were increased by less than 2-fold in the jejunum of aged KO mice (Figure 7C, Supplementary Figure S11C, S11D), and O-PLS-DA of the two aged jejunum groups yielded a T1 score of only 6.1%. The permutation test still indicated a significant separation of the two groups, with R^2Y at 0.992 ($p = 0.01$) and Q^2 at 0.707 ($p = 0.01$) (Figure 7F). S-PLS-DA resulted in the overlap of the 4 clusters, (Figure 7G), consistent with a low level of metabolic changes in the aging and PEMT-deficient jejuna. In addition, we only observed increased uridine levels in the aging profile of PEMT KO jejuna (Supplementary Figure S15E, S15F).

Surprisingly, PEMT deficiency strongly affected the metabolic profile of the ileum in young mice. There, we found increased levels of glutamate, threonine, glycine, histidine, tryptophan, isoleucine, valine, phenylalanine, glycerol, tyrosine, hypoxanthine, asparagine, uracil, glutamine, leucine, methionine, and lysine by less than 2-fold, accompanied by decreased inosine (> 4-fold) and fumarate (≈ 2-fold) (Figure 8A, Supplementary Figures S12A, S12B). The O-PLS-DA plot showed a separation of the two groups with a T1 score of 38% (Figure 8B). The permutation test showed R^2Y at 0.976 ($p < 0.01$) and Q2 at 0.923 ($p < 0.01$) (Figure 8E), further demonstrating a significant separation. Metabolism of aged KO

 doi:10.20944/preprints202208.0159.v1

tissues seems less affected, as the corresponding volcano plot showed only a slight increase in hypoxanthine and ethanolamine, and lower concentrations of allantoin, fumarate, dimethylamine, and uridine, with only allantoin showing a more than 2-fold change (Figure 8C, Supplementary Figure S13A, S13B). Group clustering on the O-PLS-DA plot with a T score of 14.5%, along with a permutation test resulting an R^2Y at 0.853 ($p < 0.01$) and a Q2 at 0.639 ($p = 0.01$), indicated a low predictive power despite a significant separation of the 2 groups (Figure 8D, 8F). Clusters of all four groups on the S-PLS-DA plot showed a consistent result with the marked metabolic alteration in the young tissues. In accordance, enrichment analysis by ORA revealed that metabolic changes in the ilea of young PEMT KO mice compared to WT mice was associated to 9 pathways (ammonia recycling, phenylalanine and tyrosine metabolism, purine metabolism, aspartate metabolism, urea cycle, glycine and serine metabolism, valine, leucine and isoleucine degradation, beta-alanine metabolism and alanine metabolism), whereas no metabolic pathways were significantly associated to the metabolic change in the aged ileum of PEMT KO mice in comparison to their WT counterparts. This indicates an essential role of PEMT in regulating metabolic homeostasis in the young ileum that decreases with aging. Aging of KO ileum is associated with the significant decrease in the levels of multiple metabolites, in line with their increase in the young KO ileum (Supplementary Figure S15G, S15H).

To summarize all differences in the metabolome between all tissues studied, we created a heatmap based on all quantified metabolites (Figures 9, 10). In line with previous observations [52], we found higher concentrations of amino acids in the metabolome of the three intestinal segments, and higher concentrations of tricarboxylic acid cycle (TCA cycle)- and lipid-associated metabolites in adipose tissues, as well as higher levels of amino acid derivatives in plasma and skeletal muscle. This further demonstrates the consistency of our data and the precision and robustness of the NMR-based metabolomic profiling approach.

3.5. Figures

 doi:10.20944/preprints202208.0159.v1

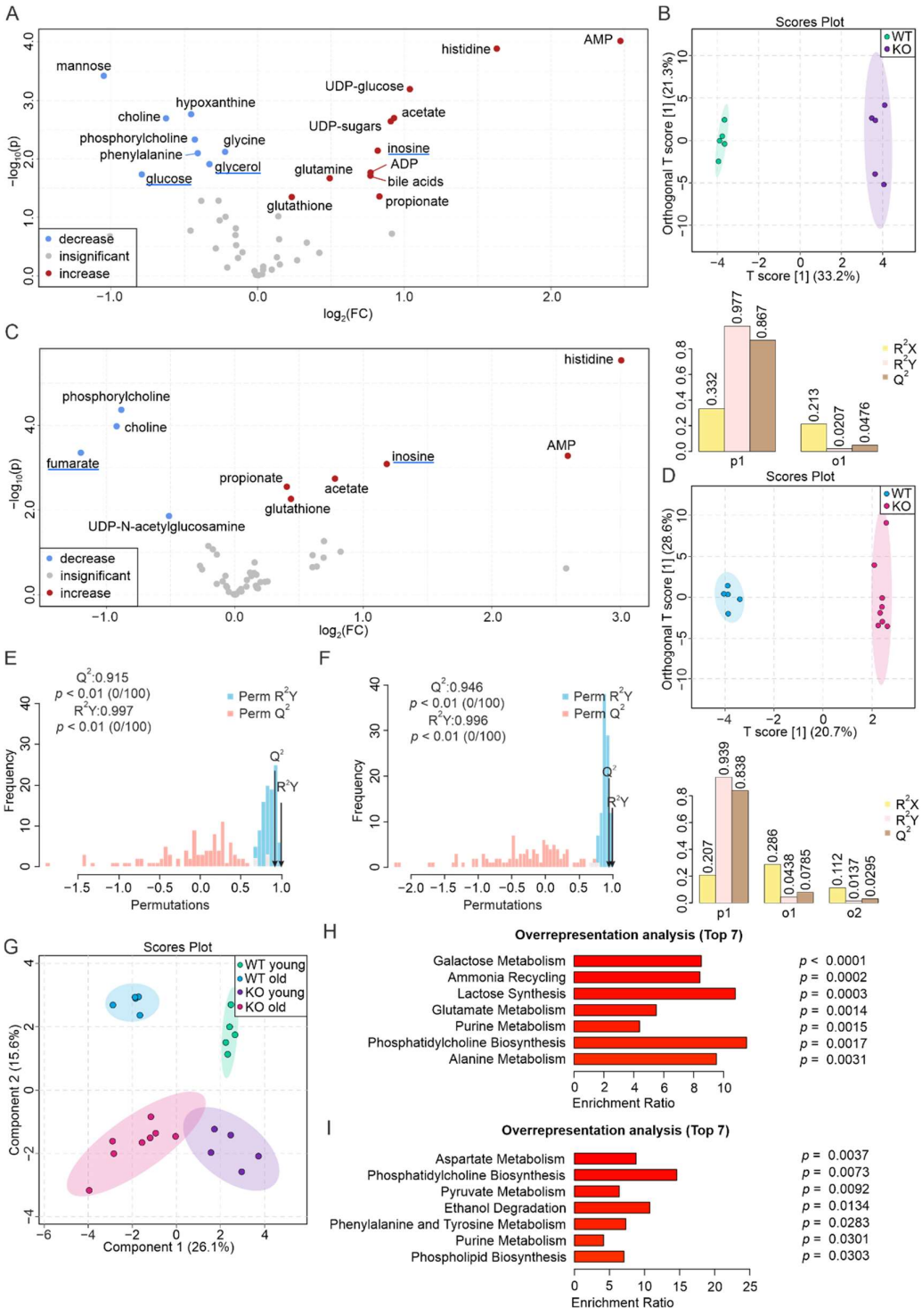

Figure 1. Drastic alteration of liver metabolome as a consequence of PEMT deficiency. (A) Volcano plot showing the differences in metabolite levels between WT and PEMT KO livers from young mice (normalization was performed for each pairwise comparison). Red and blue dots represent significantly increased and decreased metabolites ($p < 0.05$),

 doi:10.20944/preprints202208.0159.v1

respectively, whereas grey dots represent metabolites with insignificant changes ($p > 0.05$). Blue and red underlines indicate aging biomarker(s) whose concentration(s) decrease and increase in the WT aged liver, respectively, also in (C). (B) O-PLS-DA plot of WT (n=5, green) and KO (n=5, purple) liver samples from young mice (upper panel) and predictive capability of the first predictive component (p1) and the first orthogonal component (o1) with cross-validation coefficients R^2X, R^2Y, and Q^2 (lower panel). (C) Volcano plot showing differences in the abundance of metabolites between WT and PEMT KO livers from aged mice. (D) O-PLS-DA plot of WT (n=5, blue) and KO (n=8, pink) liver samples from aged mice (upper panel) and predictive capability of p1 and o1 with cross-validation coefficients R^2X, R^2Y, and Q^2 (lower panel). (E) Histogram for the permutation test of the samples in (B) and (F) of the samples in (D) with permutation number n = 100, respectively. (G) S-PLS-DA plot showing the clustering of samples from the four liver groups, with green, blue, purple, and pink corresponding to WT young, WT old, KO young, and KO old, respectively. (H) Overrepresentation analysis of top 7 pathways associated to significantly altered metabolites in livers of young mice (A), and (I) overrepresentation analysis of top 7 pathways associated with significantly altered metabolites in aged mice (C) with all pathways $p < 0.05$.

 doi:10.20944/preprints202208.0159.v1

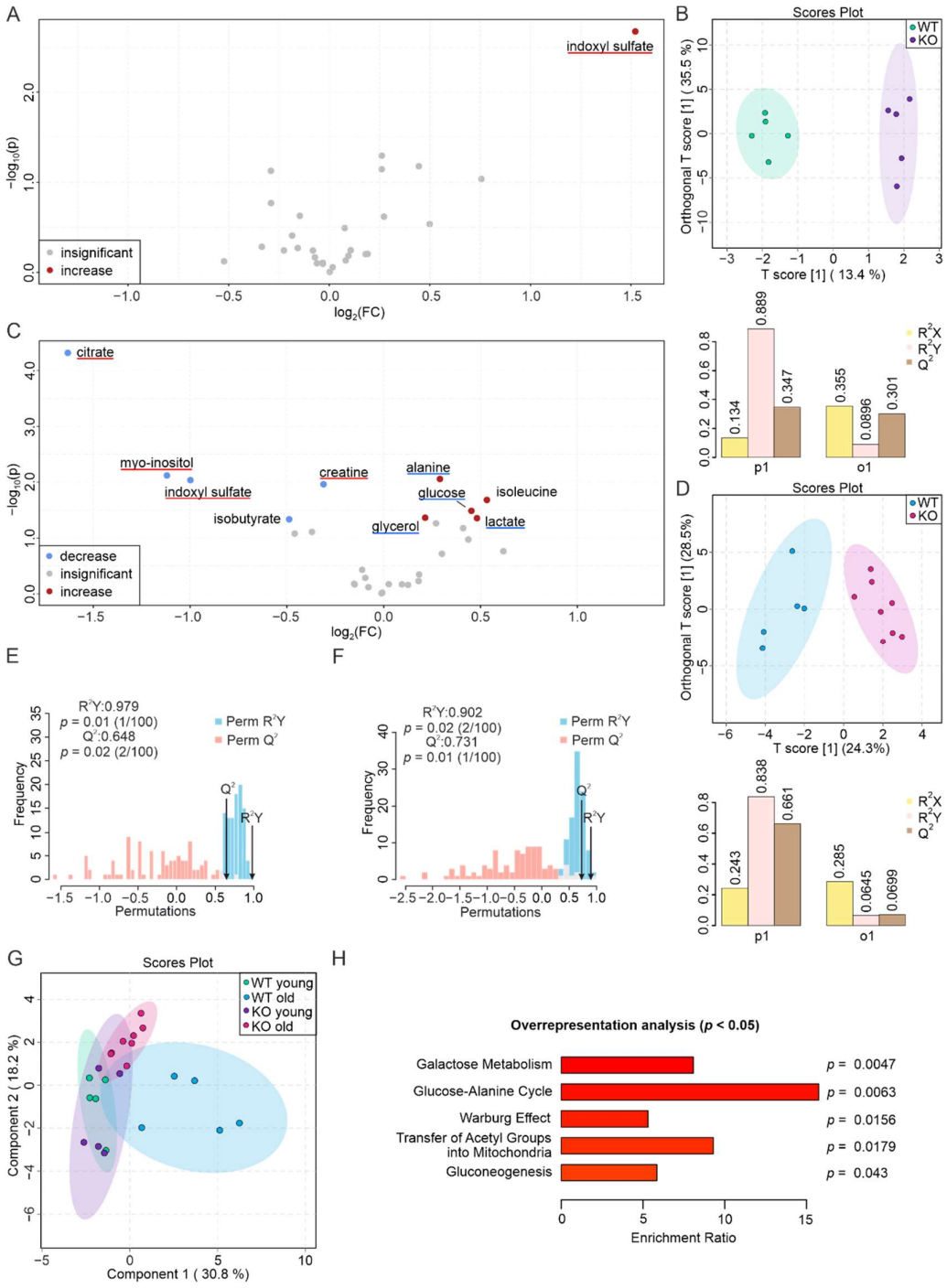

Figure 2. PEMT deficiency affects plasma metabolites upon aging. (A) Volcano plot showing differences in the abundance of metabolites between WT and PEMT KO plasma from young mice. Red dot represents a significantly increased metabolite ($p < 0.05$). Grey dots denote metabolites with insignificant changes ($p > 0.05$). Blue and red underlines indicate aging biomarker(s) whose concentration(s) decrease and increase in the WT aged plasma, respectively, also in (C). (B) O-PLS-DA plot of WT (n=5, green) and KO (n=5, purple) plasma samples from young mice (upper panel), and permutation of the first predictive component (p1) and the first orthogonal component (o1) with cross-validation coeffi-

 doi:10.20944/preprints202208.0159.v1

cients R^2X, R^2Y, and Q^2 (lower panel). (C) Volcano plot showing differences in the abundance of metabolites between WT and PEMT KO plasma from aged mice. Red and blue dots correspond to significantly increased and decreased metabolites, respectively. Grey dots denote metabolites with insignificant changes. (D) O-PLS-DA plot of WT (n=5, blue) and KO (n=8, pink) plasma samples from aged mice (upper panel), and permutation of p1 and o1 with cross-validation coefficients R^2X, R^2Y, and Q^2 (lower panel). (E) Histogram showing the permutation test of samples in (B) and (F) samples in (D) with permutation number n = 100, respectively. (G) S-PLS-DA plot showing the clustering of samples from the 4 plasma groups, with green, blue, purple, and pink corresponding to WT young, WT old, KO young, and KO old, respectively. (H) Overrepresentation analysis of pathways associated to significantly altered metabolites in the plasma of aged mice (C), with all pathways $p < 0.05$.

 doi:10.20944/preprints202208.0159.v1

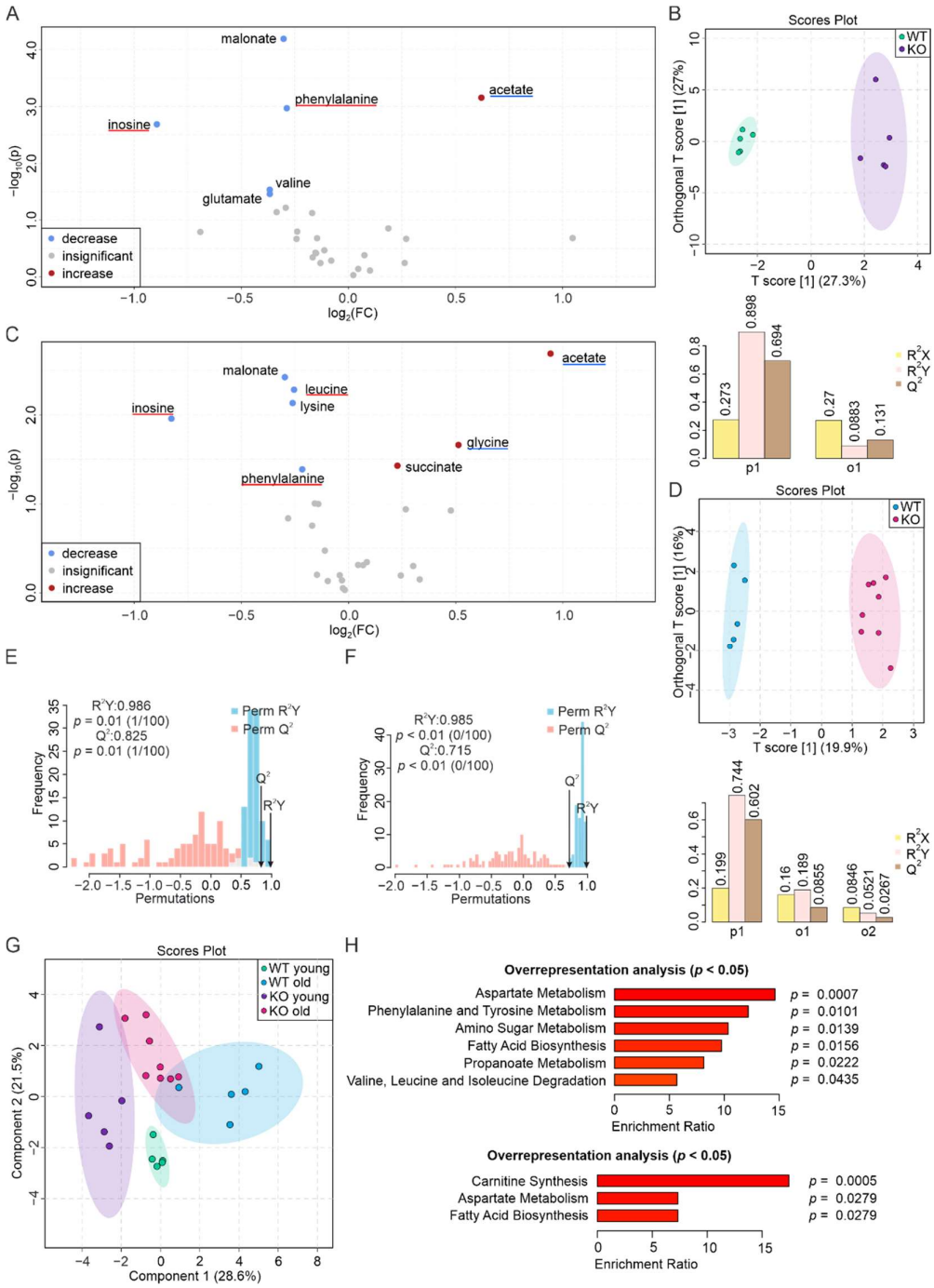

Figure 3. Contrasting metabolic changes in skeletal muscle upon PEMT deficiency and aging. (A) Volcano plot indicating increased (red), insignificantly changed (grey) and decreased (blue) metabolites in the PEMT KO skeletal muscle of young mice, in comparison to their WT counterparts. Underlines indicate aging biomarker(s) whose concentration(s) decrease (blue) and increase (red) in the WT aged skeletal muscle, also in (C). (B) O-PLS-DA plot clustering WT (n=5, green) and KO (n=5, purple) skeletal muscle samples from young mice (upper panel), along with the permutation of p1 and o1 with cross-validation coefficients R^2X, R^2Y, and Q^2 (lower panel). (C) Volcano plot indicating increased (red), insignificantly changed (grey) and decreased (blue) metabolites in the PEMT KO skeletal

 doi:10.20944/preprints202208.0159.v1

muscle of aged mice, in comparison to its WT counterpart. (D) O-PLS-DA plot clustering WT (n=5, blue) and KO (n=8, pink) skeletal muscle samples from aged mice (upper panel), and permutation of p1, o1 and o2 (second predictive component) with cross-validation coefficients R^2X, R^2Y, and Q^2 (lower panel). (E) Histogram showing the permutation test of samples in (B) and (F) samples in (D) with permutation number n = 100, respectively. (G) S-PLS-DA plot of 4 skeletal muscle groups, with green, purple, blue, and pink corresponding to WT young, KO young, WT old, and KO old, respectively. (H) Overrepresentation analysis of pathways associated to significantly changed metabolites in the skeletal muscle of young mice (A), with all pathways $p < 0.05$. (I) Overrepresentation analysis of pathways associated to significantly changed metabolites in the skeletal muscle of aged mice (C), with all pathways $p < 0.05$.

Preprints (www.preprints.org) | NOT PEER-REVIEWED | Posted: 8 August 2022 doi:10.20944/preprints202208.0159.v1

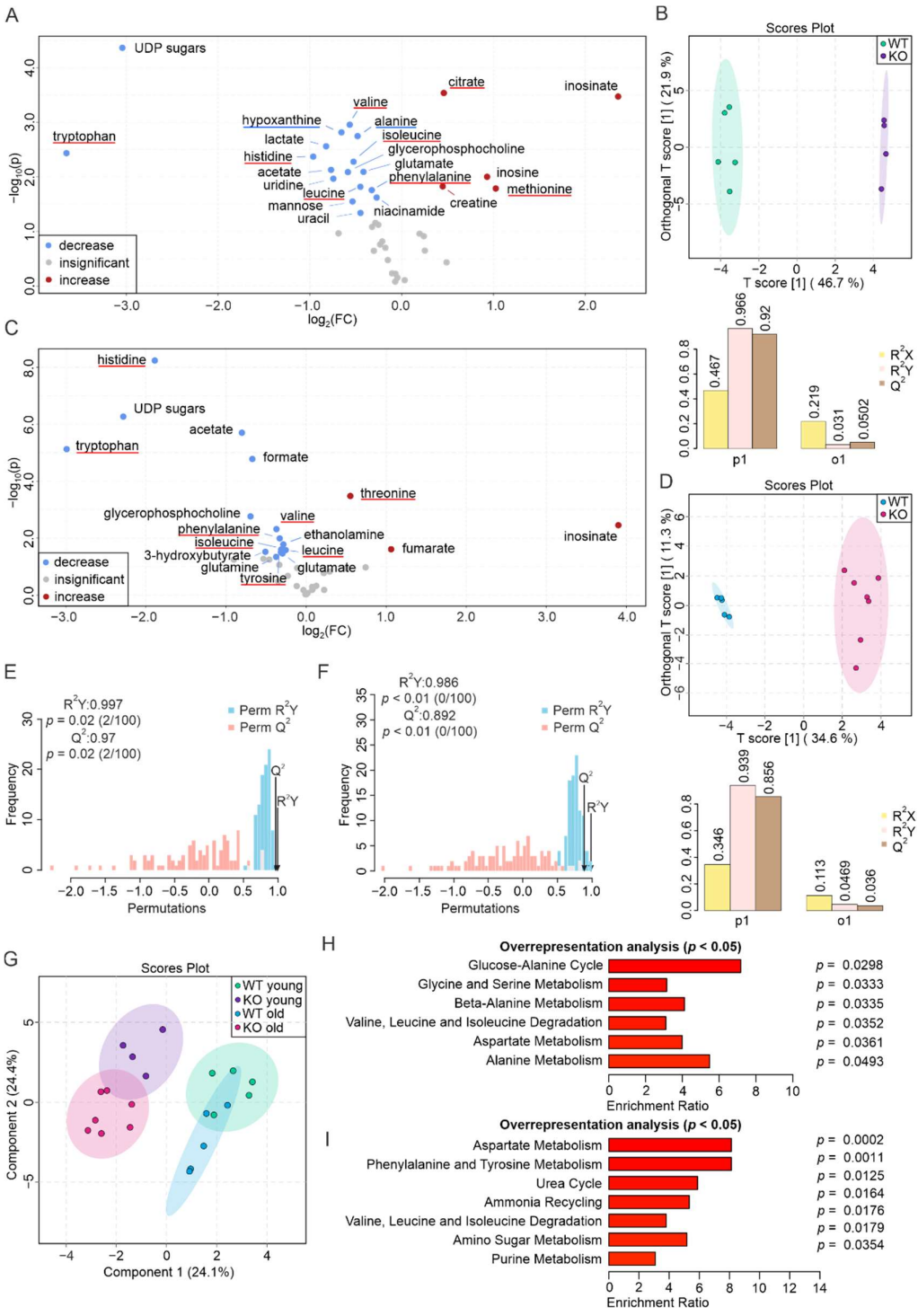

Figure 4. Metabolic alterations in the PEMT KO BAT from young and aged mice. (A) Volcano plot showing differences in the metabolite abundance between WT and PEMT KO BAT from young mice. Red and blue dots correspond to increased and decreased metabolites, respectively. Grey dots denote metabolites with insignificant changes. Blue and red underlines indicate aging biomarker(s) whose concentration(s) decrease and increase in the WT aged BAT, respectively, also in (C). (B) O-PLS-DA plot of WT (n=5, green) and

 doi:10.20944/preprints202208.0159.v1

KO (n=4, purple) BAT samples from young mice (upper panel), and cross-validation coefficients R^2X, R^2Y, and Q^2 of p1 and o1 (lower panel). (C) Volcano plot showing differences in the abundance of metabolites between WT and PEMT KO BAT from aged mice. (D) O-PLS-DA plot (upper panel) and cross-validation coefficients R^2X, R^2Y, and Q^2 of p1 and o1 (lower panel) of WT (n=5, blue) and KO (n=7, pink) BAT samples from aged mice. (E) Histogram of permutation test for samples in (B) and (F) samples in (D) with permutation number n = 100, respectively. (G) S-PLS-DA plot of the 4 BAT groups, with green, purple, blue, and pink corresponding to WT young, KO young, WT old, and KO old, respectively. (H) Overrepresentation analysis of pathways associated to significantly changed metabolites in the BAT of young mice (A) and (I) of aged mice (C), with all pathways $p < 0.05$.

 doi:10.20944/preprints202208.0159.v1

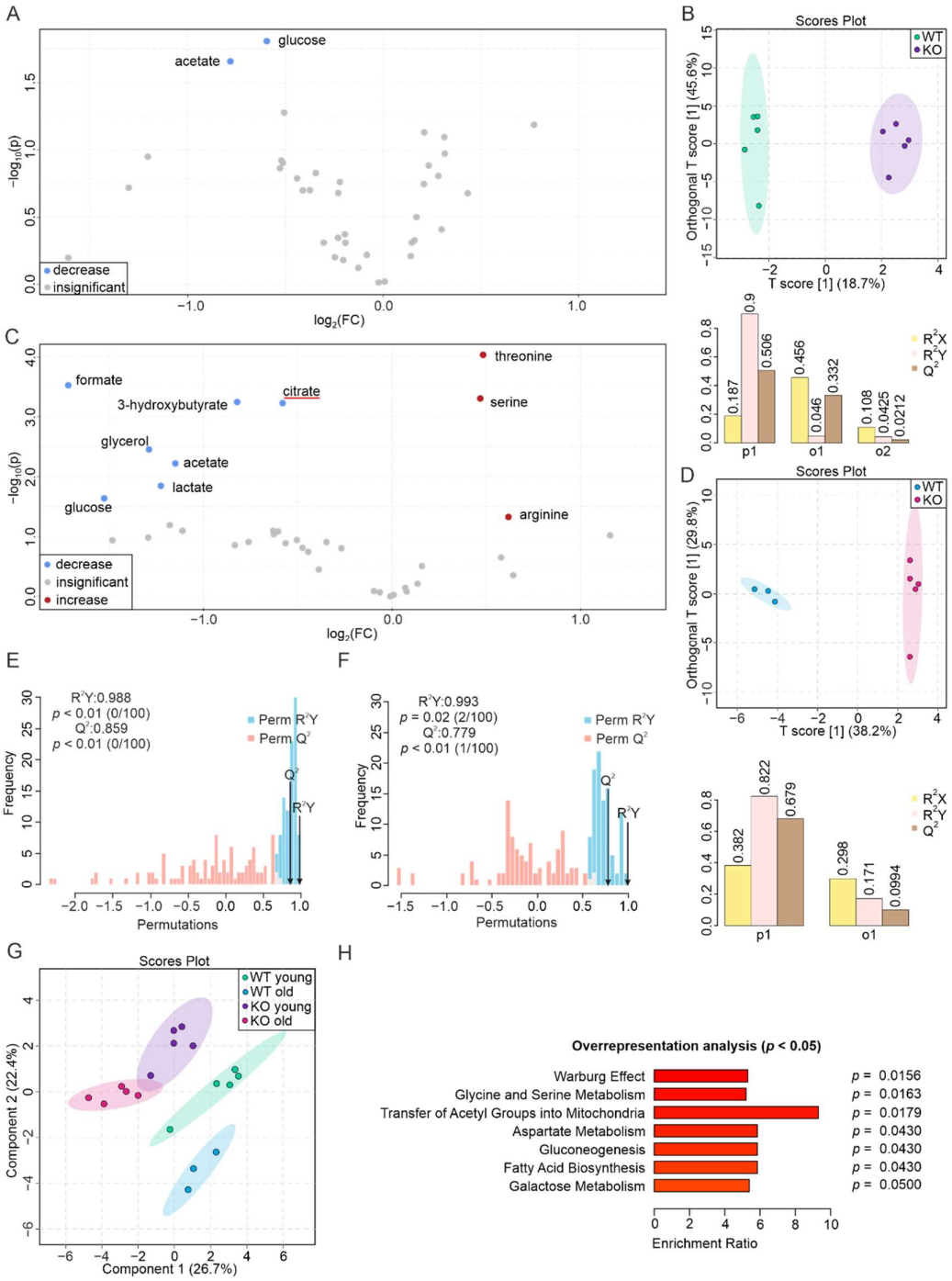

Figure 5. Metabolic alterations in WAT of young and aged PEMT KO mice. (A) Volcano plot showing differences in the metabolic profiles of WT and PEMT KO WAT from young mice. Red, blue, and grey dots indicate significantly increased, decreased, and insignificantly changed metabolites, respectively. (B) O-PLS-DA plot of WT (n=5, green) and KO (n=5, purple) WAT samples from young mice (upper panel), and predictive power of p1, o1 and o2 with cross-validation coefficients R^2X, R^2Y, and Q^2 (lower panel). (C) Volcano plot showing differences in the metabolic profiles of WT and PEMT KO WAT from aged mice. Red underline indicates an aging biomarker whose concentration increases in the aged WT WAT. (D) O-PLS-DA plot of WT (n=3, blue) and KO (n=5, pink) WAT samples

 doi:10.20944/preprints202208.0159.v1

from aged mice (upper panel), and predictive power of p1 and o1 with cross-validation coefficients R^2X, R^2Y, and Q^2 (lower panel). (E) Permutation test of samples in (B) and (F) samples in (D) with permutation number n = 100, respectively. (G) S-PLS-DA plot of the 4 WAT groups, with green, purple, blue, and pink corresponding to WT young, KO young, WT old, and KO old, respectively. (H) Overrepresentation analysis of pathways associated to significantly changed metabolites in the WAT of aged mice (C), with all pathways $p < 0.05$.

 doi:10.20944/preprints202208.0159.v1

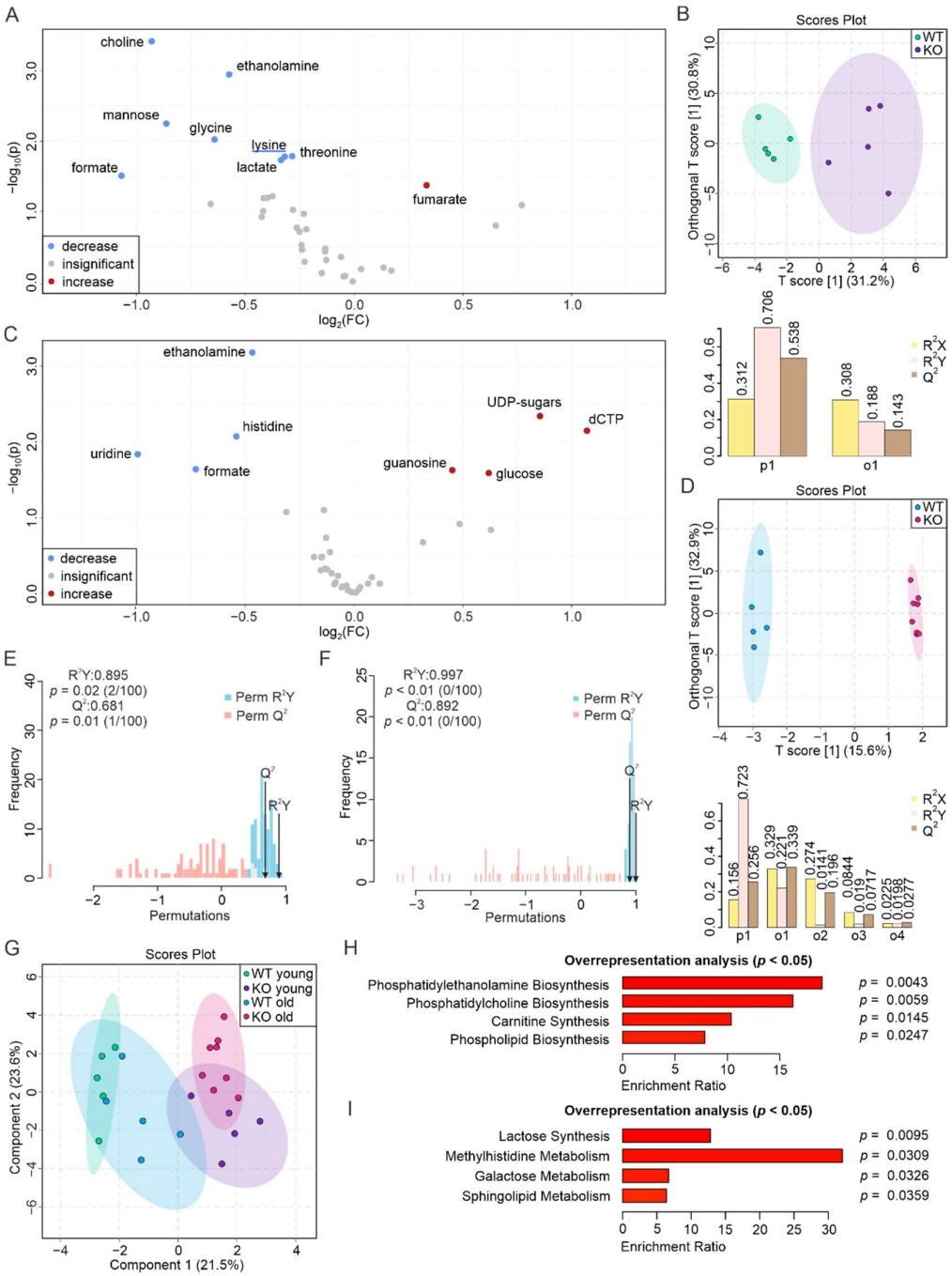

Figure 6. PEMT deficiency affects metabolic stability of young and old duodena. (A) Volcano plot showing differences in the metabolite concentrations between WT and PEMT KO duodenum from young mice. Red and blue corresponds to significantly increased and decreased metabolites, respectively. Grey dots denote metabolites with insignificant changes. Blue underline indicates an aging biomarker whose concentration decreases in the aged WT duodenum. (B) O-PLS-DA plot of WT (n=5, green) and KO (n=5, purple) duodenum samples from young mice (upper panel), and predictive power of p1 and o1 with cross-validation coefficients R^2X, R^2Y, and Q^2 (lower panel). (C) Volcano plot showing differences in the metabolite concentrations between WT and PEMT KO duodena from aged mice. (D) O-PLS-DA plot of WT (n=5, blue) and KO (n=8, pink) duodenum

Preprints (www.preprints.org) | NOT PEER-REVIEWED | Posted: 8 August 2022 doi:10.20944/preprints202208.0159.v1

samples from aged mice (upper panel), and predictive power of p1 and four orthogonal components (o1, o2, o3, o4) with cross-validation coefficients R^2X, R^2Y, and Q^2 (lower panel). (E) Histogram of permutation test for samples in (B) and (F) for samples in (D) with permutation number n = 100, respectively. (G) S-PLS-DA plot of the 4 duodenum groups, with green, purple, blue, and pink corresponding to WT young, KO young, WT old, and KO old, respectively. (H) Overrepresentation analysis of pathways associated to significantly changed metabolites in the duodenum of (A) young mice and (C) aged mice, with all pathways $p < 0.05$.

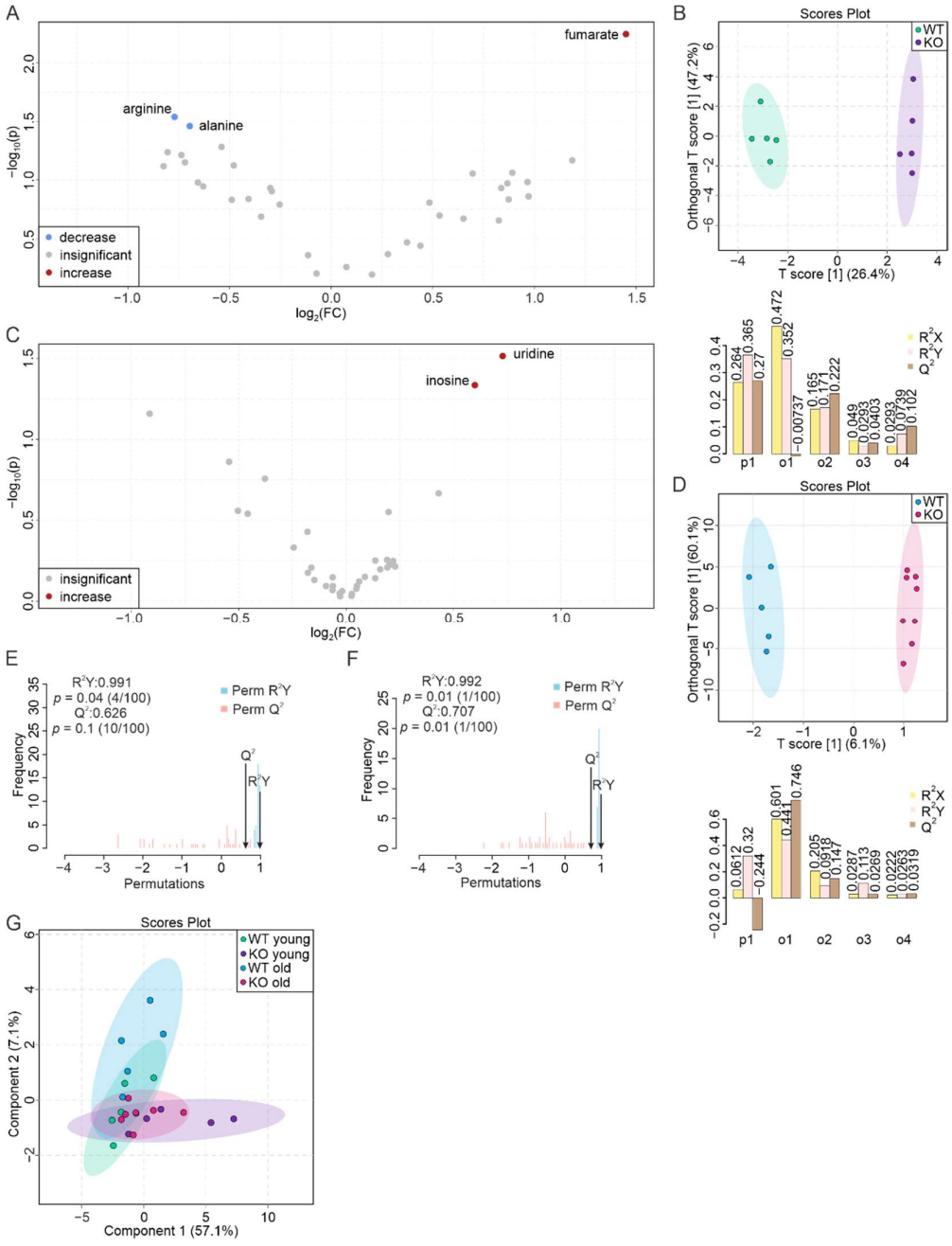

 doi:10.20944/preprints202208.0159.v1

Figure 7. Jejunal metabolites are hardly affected by ageing or PEMT deficiency. (A) Volcano plot showing differences in the metabolic profiles of WT and PEMT KO jejunum from young mice. Red and blue corresponds to significantly increased and decreased metabolites, respectively. Grey dots correspond to metabolites with insignificant changes. (B) O-PLS-DA plot of WT (n=5, green) and KO (n=5, purple) jejunum samples from young mice (upper panel), and prediction power of p1 and four orthogonal components (o1, o2, o3, o4) with cross-validation coefficients R^2X, R^2Y, and Q^2 (lower panel). (C) Volcano plot showing differences in the metabolic profiles of WT and PEMT KO jejunum from aged mice. Red dots represent significantly increased metabolites. Grey dots denote metabolites with insignificant changes. (D) O-PLS-DA plot of WT (n=5, blue) and KO (n=8, pink) jejunum samples from aged mice (upper panel), and predictive power of p1 and four orthogonal components (o1, o2, o3, o4) with cross-validation coefficients R^2X, R^2Y, and Q^2 (lower panel). (E) Histogram showing permutation test of samples in (B) and (F) of samples in (D) with permutation number n = 100, respectively. (G) S-PLS-DA plot of the 4 jejunum groups, with green, purple, blue, and pink corresponding to WT young, KO young, WT old, and KO old, respectively.

 doi:10.20944/preprints202208.0159.v1

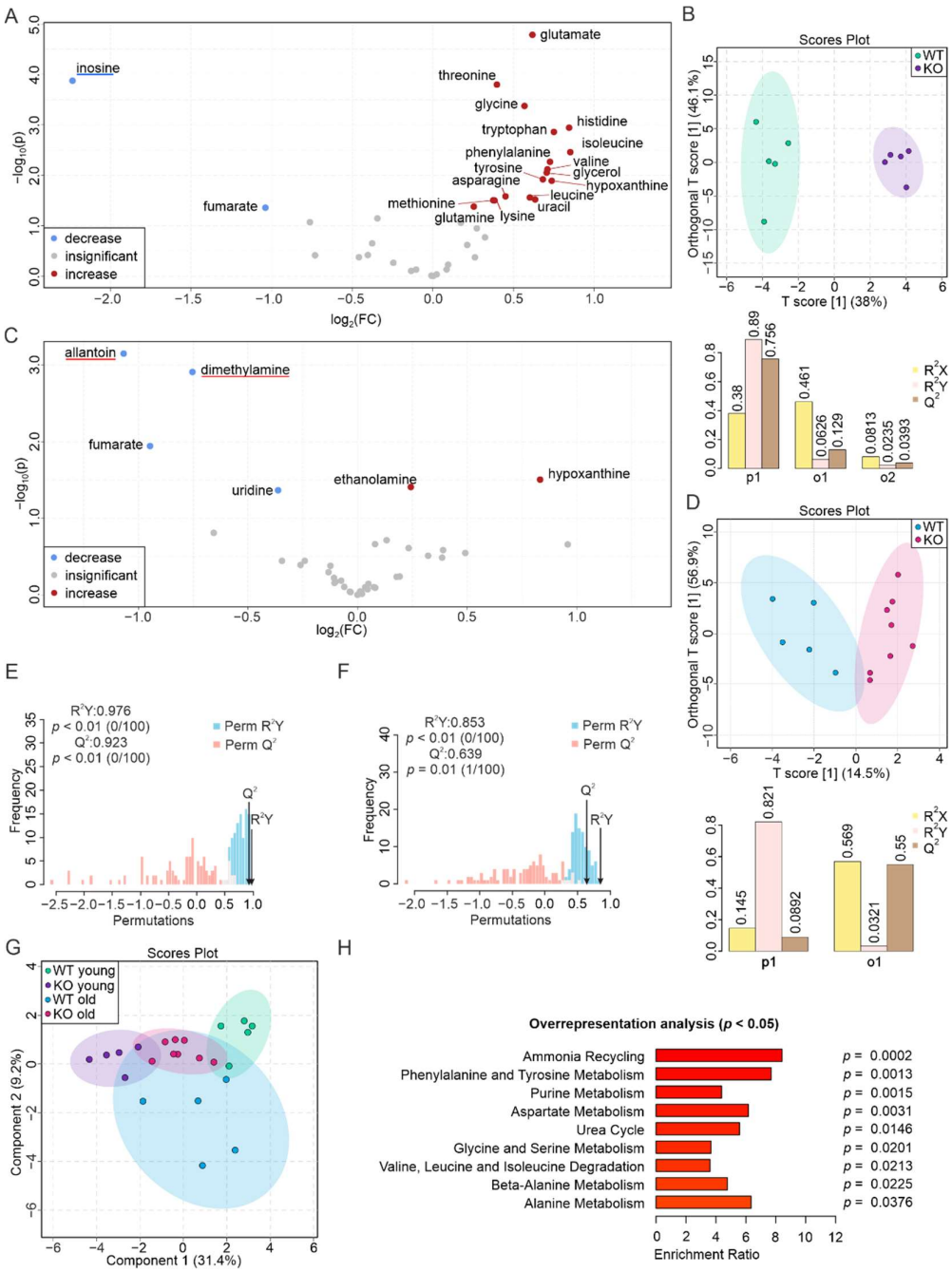

Figure 8. PEMT deficiency severely affects the metabolome of young ilea. (A) Volcano plot showing differences in the metabolite concentrations between WT and PEMT KO ileum from young mice. Red, blue and grey dots correspond to significantly increased, decreased and insignificantly changed metabolites, respectively. Blue underline indicates an aging biomarker whose concentration decreases upon aging in the WT ileum. (B) O-PLS-DA plot of WT (n=5, green) and KO (n=5, purple) ileum samples from young mice (upper panel), and cross-validation coefficients R^2X, R^2Y, and Q^2 of p1, o1 and o2(lower panel). (C) Volcano plot showing differences in metabolite concentrations between WT and PEMT KO ilea from aged mice. Red underlines highlight ageing biomarkers whose concentrations increase upon aging in WT ilea. (D) O-PLS-DA plot of WT (n=5, blue) and KO (n=8, pink) ileum samples from aged mice (upper panel), and cross-validation coefficients

 doi:10.20944/preprints202208.0159.v1

R^2X, R^2Y, and Q^2 of p1 and o1 (lower panel). (E) Histogram showing permutation test of samples in (B) and (F) of samples in (D) with permutation number n = 100, respectively. (G) S-PLS-DA plot of the 4 ileum groups, with green, purple, blue, and pink corresponding to WT young, KO young, WT old, and KO old, respectively. (H) Overrepresentation analysis of pathways associated to significantly changed metabolites in the ileum of young mice (A), with all pathways $p < 0.05$.

 doi:10.20944/preprints202208.0159.v1

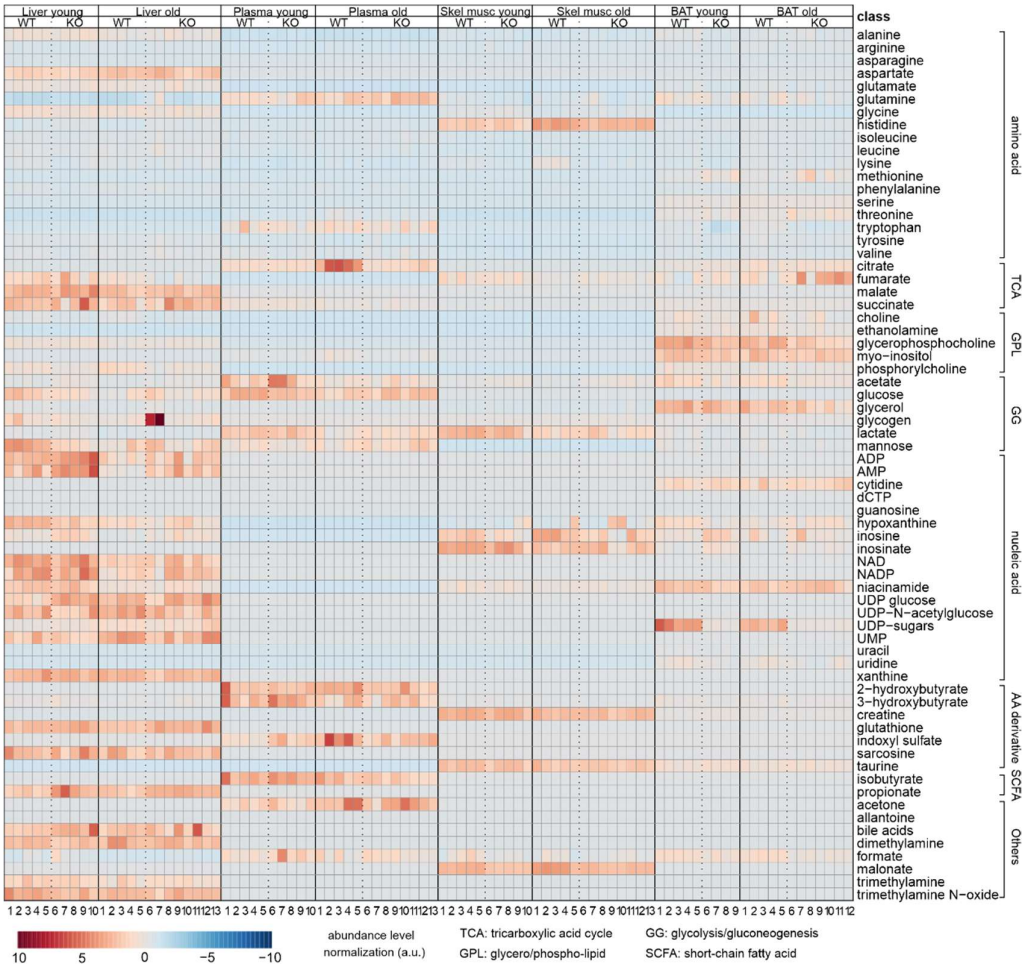

Figure 8. Heatmap of the quantified metabolites in liver, plasma, skeletal muscle, and BAT. The respective tissues, age of mice, and genotypes are indicated on top, metabolites at right. Sample numbers for each pairwise comparison is given below (young, n = 9-10; old, n = 8-13). Each single cell represents a relative abundance of the corresponding metabolite compared to the average, as previously described [52]. Within the same tissue data from all 4 groups are normalized to enable the comparison, from which metabolites at higher concentrations are in red, metabolites at lower concentrations are in blue.

Preprints (www.preprints.org) | NOT PEER-REVIEWED | Posted: 8 August 2022 doi:10.20944/preprints202208.0159.v1

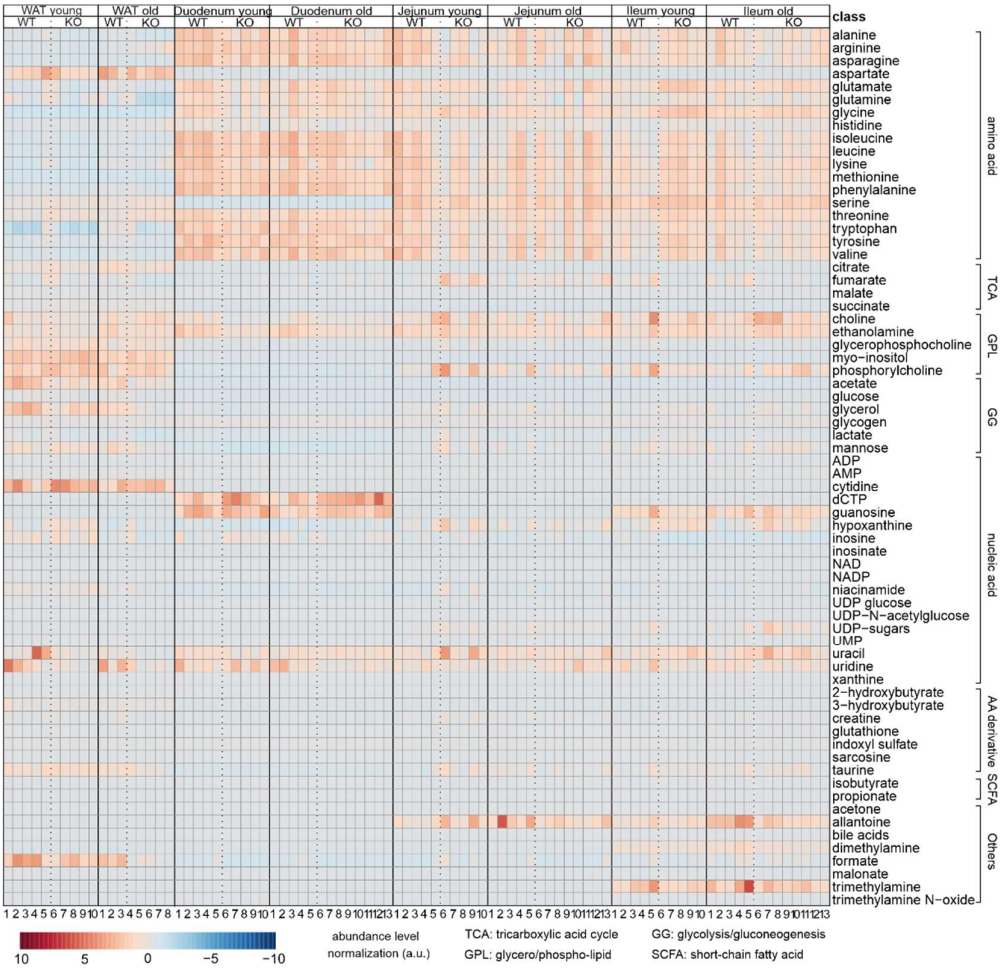

Figure 9. Heatmap of metabolites identified in WAT, duodenum, jejunum, and ileum. The respective tissues, age of mice, and genotypes are indicated on the top, metabolites on the right. Total samples numbers are given below. Increased metabolites are in red and decreased metabolites are in blue.

4. Discussion

In this study, the metabolome of liver, plasma, skeletal muscle, BAT, WAT, and intestine (duodenum, jejunum, ileum) from young and aged WT and PEMT KO mice was investigated and revealed a plethora of metabolic changes due to the interference between aging and PEMT deficiency. The metabolomes of all PEMT KO tissues except jejunum were strongly affected, demonstrating that global PEMT deficiency has profound systemic consequences. This finding was consistent with the importance of PC levels and PC/PE ratios in the individual tissues in maintaining proper function of liver, intestine and skeletal muscle [19].

In recent decades, consequences of PEMT deficiency have been extensively studied [39,40,43,60,61], but the underlying molecular mechanisms are still incompletely understood. Here, we provide the first systematic metabolomic-based characterization of both tissue-specific and age-dependent metabolic alterations in PEMT KO mice. Based on the

 doi:10.20944/preprints202208.0159.v1

outline of the metabolomic landscape uncovered in this study, we delineate (i) the metabolic changes due to the KO of PEMT, (ii) secondary effects to maintain tissue homeostasis and to cover the requirement of PC in response to the lack of functional PEMT, and (iii) indirect effects not directly linked to PL metabolism, but likely triggered by the availability of PCs and PEs.

Since PC is essential for the secretion of hepatic VLDL, the lack of choline leads to hepatic triacylglycerol (TG) accumulation [19,62,63]. Furthermore, loss-of-function mutation of PEMT in humans may be associated with non-alcoholic fatty liver disease (NAFLD) as a possible consequence of altered PC synthesis and increased TG accumulation [64]. Expectedly, we identified important changes in various metabolic pathways from KO liver.

PEMT deficiency in the livers of young mice resulted in a drastic change of their metabolome, whereas the majority of detected metabolites remained unchanged in the livers of aged KO mice. Increased levels of AMP, histidine, inosine, acetic acid, propionate, and glutathione, as well as decreased phosphorylcholine and choline levels were found to be comparable in both young and aged livers, suggesting that they are age-independent. This indicated that liver metabolism is largely stabilized during aging, possibly due to an increased supply of PC in aged mice.

Considering the changes in individual metabolites, the decrease of choline and phosphorylcholine are attributable to secondary effects of PEMT deficiency, likely due to a compensatory increase in PC synthesis through the CDP-choline pathway. Such a mechanism has already been identified in previous studies using both choline and phosphorylcholine as precursors of PCs [31,65]. Indirect consequences, such as increases of AMP in livers of young and old KO mice, together with increase of ADP in young KO mice, indicate a change in the ratio of ADP/ATP and AMP/ATP. This could result from an altered energy consumption. Interestingly, it has been previously found that PEMT deficiency results in increased ATP concentration in hepatocytes [38], which contradicts our results. The activity of uncoupling protein-2 (UCP2), a regulator of ATP concentration in the mitochondria [66], could be responsible for this discrepancy. The levels of UCP2 change differently in PEMT KO BAT and skeletal muscle and is affected by diet [42,43,67], which might also cause the divergence in the hepatic ATP levels due to different experimental conditions.

As for amino acids, histidine is expected to be catabolized into glutamate, with the latter being a precursor for glutathione biosynthesis [68,69]. Increased levels of both histidine and glutathione in young and aged mice without a significant change in the concentration of glutamate suggested the upregulation of both histidine production and increased proteolysis for glutathione biosynthesis. In addition, the increase of glutamine in the young KO liver could alternatively account for an increased glutamate consumption [70]. However, further mechanistic studies are needed to evaluate these interpretations, and to check whether this is a side effect of increased amino acid catabolism for energy generation.

The level of glycogen in the KO liver has been found to decrease upon overnight fasting [38]. However, in the present study we observed reduced glucose level, but not glycogen, in the young KO liver. This indicates absence or reduction of gluconeogenesis upon overnight fasting (see Methods) in KO liver. Interestingly, the increase of acetate, which is likely a result of reduced conversion to acetyl-CoA [71], could represent a compensatory mechanism to restore gluconeogenesis, as dietary acetate has been demonstrated to increase glycogen concentration in rat livers [72]. We also found an increase of bile acids in young KO livers, whose main function is to facilitate digestion [73]. Overall, we observed effects of PEMT deficiency on altering various biological functions in the

 doi:10.20944/preprints202208.0159.v1

liver, which could be a result of altered PL compositions in the different compartments of the liver such as cell membranes and VLDL.

One of the main roles of plasma is to transport nutrients and metabolites, whose metabolome reflects various biological processes from different tissues [74,75]. The levels of plasma ethanolamine, choline, phosphorylcholine, and glycerophosphocholine were below the detection limits, therefore the detected changes in the metabolome are mostly indirect consequences of PEMT deficiency. In young mice, loss of PEMT solely led to an increase of plasma indoxyl sulfate, which is synthesized by cytochrome P450 and increases during aging or reduced renal clearance [52,76,77]. Interestingly, plasma of KO mice showed opposite changes in the metabolites identified in aging mice [52], suggesting that lack of PEMT could delay or reverse the corresponding age-related alterations. Among the top five metabolic pathways associated with the altered plasma metabolome from aged KO mice, four of them were related to aging biomarkers of WT plasma. These metabolic pathways are linked to myo-inositol, glucose, and glycerol. The decrease of myo-inositol in the plasma of aged KO mice indicated increased conversion to phosphatidylinositol-3-phosphate (PI3P) and increased autophagy [78,79]. Their elevated glucose levels are not in line with previous studies showing improved insulin sensitivity and decreased hepatic gluconeogenesis in the KO mice [38,80]. This suggest a yet unknown mechanism promoting the production of glucose. Increase of free glycerol could be due to enhanced lipolysis during overnight fasting [81]. Citrate is a component of TCA cycle and has been previously found to increase in aged WT plasma [52]. Its decrease in aged plasma of KO mice suggests that age-associated lipid metabolism could be affected. Furthermore, circulating alanine levels increase in mice with hyperglycemia and may promote elevation of plasma isoleucine concentrations [82], we observed consistent results showing concomitant increase of alanine, isoleucine, and glucose in old KO mice.

Given that PEMT acts mainly in the liver and its expression in muscle tissues is extremely low [53,61], it is most likely that the observed metabolic changes in skeletal muscle are due to secondary effects of PEMT deficiency. The previously described aging metabolic phenotype of skeletal muscle from WT mice was consistent with decreased muscle function and activity [52]. Changes in the levels of metabolites including lactate, leucine, phenylalanine and glucose during aging of WT skeletal muscle [52] are not found in aged KO skeletal muscle. These metabolites are linked to the energy consumption, whose absence may indicate a beneficial effect of PEMT deficiency on muscle aging by muscle activity recovery, as reported by an increased metabolic rate of the skeletal muscle in PEMT deficiency [60]. The resting metabolic rate declines with age [83], improved resting metabolic rate by PEMT suppression may reverse age-related metabolic alterations. Considering the conditions under which the metabolic rate should increase [60], the decrease of malonate might potentiate the consumption of succinate. Paradoxically, we observed elevated concentrations of succinate, suggesting an increased conversion of succinyl-CoA to succinate as a result of increased energy expenditure via the TCA cycle [84].

Taken together, PEMT deficiency increases energy metabolism of skeletal muscle, which is known to decrease during aging [52]. However, the effects of aging and PEMT deficiency do not oppose and counteract each other. Moreover, PEMT regulates metabolites whose concentrations do not change during aging, and skeletal muscle from aged PEMT KO mice is therefore adapted to maintain homeostasis.

Lack of PEMT was shown not to impair the thermogenic capacity of BAT [42], however both our results and a previous report [61] suggested dramatic metabolic alterations of BAT upon PEMT deficiency. Of note, despite the expression of PEMT in BAT has been

 doi:10.20944/preprints202208.0159.v1

confirmed by mRNA quantification and immunoblotting [53,61], its function has been considered liver-specific and most functions of BAT are not directly regulated by locally expressed PEMT [61,85]. If PEMT expressed in BAT directly converts local PE to PC, tissue homeostasis responding to PEMT deficiency might increase PC synthesis via CDP-choline pathway or decrease PC metabolism, as well as increase PE metabolism via phospholipase activities [31,86,87], causing a decrease of choline and increase of ethanolamine levels. However, we only observed a decrease in ethanolamine in KO BAT, whereas choline levels remained unchanged. However, in both young and aged KO BAT we observed the decrease of glycerophosphocholine, which is a potential source of choline in yeast [88] and the product of PC catabolism in various cells [89,90]. This could indicate that a homeostatic process increasing PC production is taken place, but through the consumption of glycerophosphocholine instead of choline.

As for indirect effect of PEMT deficiency in BAT, the decrease in the levels of metabolites from KO BAT manifest as an age-independent manner (Figure S8C), and most aging biomarkers whose levels are increased during aging are found in both WT and KO BAT. This indicates that PEMT deficiency causes age-independent changes in the metabolome of BAT and *vice versa*. Among decreased metabolites in the KO BAT, BCAAs are known to supply BAT thermogenesis, and glutamate is a byproduct of BCAA catabolism [91,92]. Taking together the decrease of acetate, which is an inhibitor of thermogenesis in BAT [93], our results indicate a slight increase of energy consumption in the KO BAT.

WAT is responsible for lipid storage and endocrine secretion, it may acquire a thermogenic function upon browning, and our previous studies have shown that its metabolism changes little during aging [52,94,95]. PEMT deficiency resulted in decreased lipogenesis, which may explain resistance to high fat diet-induced obesity [96]. We were only able to detect metabolic changes in aged PEMT KO mice, indicating that only combined aging and PEMT deficiency can significantly alter the abundance of several metabolites. Upon decreased lipogenesis that occurs in WAT, the decrease of glucose in both young and aged KO WAT may be a result of reduced gluconeogenesis or increased utilization [38]. In agreement, the increase of serine in WAT from aged KO mice could indicate an increased conversion from glucose [97]. In the metabolome of WAT from aged PEMT KO mice, the decreased levels of glycerol could be one of the reason for the decreased lipogenesis [96]. Increased amounts of glycerol in plasma could be released from WAT, as a product of elevated basal lipolysis of triglycerides [21,81]. Citrate is a component of the TCA cycle [71], whose decrease may be due to an increased flux through the TCA cycle [38], in combination with a higher conversion of acetyl-CoA. This is consistent with the decrease in glucose and acetate, which are the possible precursors of acetyl-CoA [98]. Interestingly, the concentration of citrate is increased in the plasma of aged KO mice, as well as in young KO BAT, but remains unchanged in aged KO BAT. This could result from the export of citrate in the plasma from both BAT and WAT in aged KO mice. Overall, the observations in WAT are consistent with decreased lipogenesis and fat accumulation, in line with previous studies [96].

Biliary PC solubilizes dietary lipids in the small intestine and facilitates their absorption [19,99]. The secretion rate of biliary PC does not differ between WT and PEMT KO mice [100]. However, PEMT KO affects Na^+ absorption and subsequent bile acid re-absorption in the small intestine [101] by an as yet unknown mechanism. Despite its involvement in nutrient absorption, our previous study identified the duodenum as a tissue without significant metabolic alterations during aging [52]. Here, we observed only age-dependent metabolic changes in the duodenum of PEMT KO mice. It has been found that small intestine acquires PC from diet in rat [102]. Thus, our results may indicate the usage

 doi:10.20944/preprints202208.0159.v1

of non-negligeable amounts of PC produced by liver in the duodenum, if not the entire small intestine. PEMT deficiency therefore might change PC supplies both in quantities and types of fatty acids during aging [35]. In comparison to the duodena from young WT mice, young KO animals exhibit decreased duodenal levels of choline and ethanolamine. We have identified that in both young and old mice, loss of PEMT caused a decrease in the levels of formate and ethanolamine, which are both related to gut microbiome [103-105]. The highest difference in the abundance of of metabolites between young and old PEMT KO mice is seen for glucose, UDP-sugars, and mannose, indicating indirect, age-related effects of PEMT deficiency on carbohydrate metabolism.

We observed only modest alterations in the jejunal metabolome caused by the loss of PEMT, showing its stable metabolism. In line, we have previously reported jejunum as a tissue that maintains stable tissue homeostasis throughout life in mice [52]. The levels of multiple components, including fumarate, uridine, ethanolamine, glycine, lysine, threonine, histidine, and inosine, were reversely altered in the different segments of the small intestine. This could originate from different cellular metabolism, nutritional sources, or the metabolic activity of the microbiome.

Surprisingly, the ileum was one of the tissues profoundly affected by PEMT deficiency, predominantly in young mice. We observed an increase in the levels of almost all amino acids, indicating increased nutrient absorption due to changes in cellular metabolism. In both young and aged KO tissues, we identified increased concentrations of hypoxanthine, a metabolic product of inosine [106], which was concomitantly reduced in the ilea of young PEMT KO mice. As the metabolome of WT ileum also displays only few changes during aging [52], a differentiated liver-originated PC supply over age may affect all three segments of the small intestine, causing remarkable changes in the metabolome of duodenum and ileum, and fewer changes in the jejunum. Fumarate, an intermediate of the TCA cycle [71], was decreased in the PEMT KO ileum, which may be a response to altered nutrient absorption and may contribute to the recovery of normal metabolism.

Overall, our study revealed a regulatory role of PEMT in the metabolic profile of various tissues, mainly through the TCA cycle and amino acid catabolism. Consequently, it manifests partly in reversal of the aging-associated metabolic alterations in plasma and skeletal muscle, but an age-dependent homeostatic regulation in adipose tissues and intestine. Future investigations should focus on a specific tissue to demonstrate PEMT-associated pathways to reveal the change in PL composition and its biological consequences.

5. Conclusions

During this study, we performed NMR-based analyses to investigate the impact of PEMT deficiency on the metabolome of liver, plasma, skeletal muscle, adipose tissue, and small intestine from young and old mice. We identified diverse consequences in different tissues due to either the alterations in lipid uptake and transport, the compensation for the altered PC production, or various functional changes due to altered PL compositions. These responses were either age-dependent or age-independent and underline the complex metabolic role of PEMT.

Supplementary Materials: The following supporting information can be downloaded at: www.mdpi.com/xxx/s1, Figure S1-S13, reduced spectra and statistical analysis of integrated metabolites; S14, S15, aging profile of PEMT KO tissues; S16, 2D ^{1}H-^{13}C HSQC spectra showing identified metabolites.

Author Contributions: Conceptualization, Dagmar Kratky and Tobias Madl; Data curation, Qishun Zhou, Jakob Kerbl-Knapp and Tobias Madl; Formal analysis, Qishun Zhou, Fangrong Zhang and Jakob Kerbl-Knapp; Funding acquisition, Gerd Hörl, Dagmar Kratky and Tobias Madl; Investigation, Qishun Zhou, Jakob Kerbl-Knapp and Tobias Madl; Methodology, Qishun Zhou, Fangrong Zhang, Jakob Kerbl-Knapp, Melanie Korbelius, Katharina Kuentzel, Nemanja Vujic, Alena Akhmetshina, Gerd Hörl, Margret Paar, Ernst Steyrer and Dagmar Kratky; Project administration, Tobias Madl; Resources, Gerd Hörl, Ernst Steyrer, Dagmar Kratky and Tobias Madl; Software, Qishun Zhou, Fangrong Zhang, Jakob Kerbl-Knapp and Tobias Madl; Supervision, Tobias Madl; Validation, Qishun Zhou and Tobias Madl; Visualization, Qishun Zhou, Fangrong Zhang and Jakob Kerbl-Knapp; Writing – original draft, Qishun Zhou; Writing – review & editing, Qishun Zhou, Fangrong Zhang, Jakob Kerbl-Knapp, Melanie Korbelius, Katharina Kuentzel, Nemanja Vujic, Alena Akhmetshina, Gerd Hörl, Margret Paar, Ernst Steyrer, Dagmar Kratky and Tobias Madl.

Funding: T.M. was supported by Austrian Science Fund (FWF) grants P28854, I3792, DOC-130, and DK-MCD W1226; Austrian Research Promotion Agency (FFG) grants 864690 and 870454; the Integrative Metabolism Research Center Graz; the Austrian Infrastructure Program 2016/2017, the Styrian Government (Zukunftsfonds, doc.fund program); and BioTechMed-Graz (flagship project). D.K. was supported by the FWF (SFB F73, W1226, P32400, P30882, DOC 31), the Province of Styria, and the City of Graz. G.H. was supported by the city of Graz (A27102000025). F.Z. was trained within the frame of the PhD program Molecular Medicine (MolMed), Medical University of Graz and supported by Startup Fund for High-level Talents of Fujian Medical University (XRCZX2021020), and Q.Z. and A.A. were trained within the frame of the PhD program Metabolic and Cardiovascular Disease (DK-MCD), Medical University of Graz.

Institutional Review Board Statement: The study was conducted according to the guidelines of the European Directive 2010/63/EU, and approved by the Austrian Federal Ministry of Education, Science and Research.

Informed Consent Statement: Not applicable.

Data Availability Statement: The data presented in this study are available on request from the corresponding author.

In this section, please provide details regarding where data supporting reported results can be found, including links to publicly archived datasets analyzed or generated during the study. Please refer to suggested Data Availability Statements in section "MDPI Research Data Policies" at https://www.mdpi.com/ethics. If the study did not report any data, you might add "Not applicable" here.

Acknowledgments: The authors thank the Center for Medical Research, Medical University of Graz, Graz, Austria for laboratory access, and thank A. Absenger and I. Hindler (Medical University of Graz, Austria) for mice care.

Conflicts of Interest: The authors declare no conflict of interest.

References

1. de Almeida, A.J.P.O.; Ribeiro, T.P.; de Medeiros, I.A. Aging: Molecular Pathways and Implications on the Cardiovascular System. *Oxid Med Cell Longev* **2017**, *2017*, 7941563-7941563, doi:10.1155/2017/7941563.
2. Preston, J.; Biddell, B. The physiology of ageing and how these changes affect older people. *Medicine* **2021**, *49*, 1-5, doi:https://doi.org/10.1016/j.mpmed.2020.10.011.
3. López-Otín, C.; Blasco, M.A.; Partridge, L.; Serrano, M.; Kroemer, G. The hallmarks of aging. *Cell* **2013**, *153*, 1194-1217, doi:10.1016/j.cell.2013.05.039.
4. DiLoreto, R.; Murphy, C.T. The cell biology of aging. *Mol Biol Cell* **2015**, *26*, 4524-4531, doi:10.1091/mbc.E14-06-1084.

5. Moaddel, R.; Ubaida-Mohien, C.; Tanaka, T.; Lyashkov, A.; Basisty, N.; Schilling, B.; Semba, R.D.; Franceschi, C.; Gorospe, M.; Ferrucci, L. Proteomics in aging research: A roadmap to clinical, translational research. *Aging Cell* **2021**, *20*, e13325-e13325, doi:10.1111/acel.13325.
6. Adav, S.S.; Wang, Y. Metabolomics Signatures of Aging: Recent Advances. *Aging Dis* **2021**, *12*, 646-661, doi:10.14336/AD.2020.0909.
7. Stegeman, R.; Weake, V.M. Transcriptional Signatures of Aging. *J Mol Biol* **2017**, *429*, 2427-2437, doi:10.1016/j.jmb.2017.06.019.
8. Hu, H.-H.; Cao, G.; Wu, X.-Q.; Vaziri, N.D.; Zhao, Y.-Y. Wnt signaling pathway in aging-related tissue fibrosis and therapies. *Ageing Research Reviews* **2020**, *60*, 101063, doi:https://doi.org/10.1016/j.arr.2020.101063.
9. Papaconstantinou, J. Insulin/IGF-1 and ROS signaling pathway cross-talk in aging and longevity determination. *Molecular and Cellular Endocrinology* **2009**, *299*, 89-100, doi:https://doi.org/10.1016/j.mce.2008.11.025.
10. Chung, K.W. Advances in Understanding of the Role of Lipid Metabolism in Aging. *Cells* **2021**, *10*, doi:10.3390/cells10040880.
11. Johnson, A.A.; Stolzing, A. The role of lipid metabolism in aging, lifespan regulation, and age-related disease. *Aging Cell* **2019**, *18*, e13048, doi:10.1111/acel.13048.
12. Mutlu, A.S.; Duffy, J.; Wang, M.C. Lipid metabolism and lipid signals in aging and longevity. *Dev Cell* **2021**, *56*, 1394-1407, doi:10.1016/j.devcel.2021.03.034.
13. Shi, Y.; Cheng, D. Beyond triglyceride synthesis: the dynamic functional roles of MGAT and DGAT enzymes in energy metabolism. *American Journal of Physiology-Endocrinology and Metabolism* **2009**, *297*, E10-E18, doi:10.1152/ajpendo.90949.2008.
14. Vance, J.E. Phospholipid Synthesis and Transport in Mammalian Cells. *Traffic* **2015**, *16*, 1-18, doi:https://doi.org/10.1111/tra.12230.
15. Jump, D.B. Fatty acid regulation of hepatic lipid metabolism. *Current Opinion in Clinical Nutrition & Metabolic Care* **2011**, *14*.
16. van Meer, G.; Voelker, D.R.; Feigenson, G.W. Membrane lipids: where they are and how they behave. *Nat Rev Mol Cell Biol* **2008**, *9*, 112-124, doi:10.1038/nrm2330.
17. Yang, Y.; Lee, M.; Fairn, G.D. Phospholipid subcellular localization and dynamics. *Journal of Biological Chemistry* **2018**, *293*, 6230-6240, doi:10.1074/jbc.R117.000582.
18. Dai, Y.; Tang, H.; Pang, S. The Crucial Roles of Phospholipids in Aging and Lifespan Regulation. *Frontiers in Physiology* **2021**, *12*, doi:10.3389/fphys.2021.775648.
19. van der Veen, J.N.; Kennelly, J.P.; Wan, S.; Vance, J.E.; Vance, D.E.; Jacobs, R.L. The critical role of phosphatidylcholine and phosphatidylethanolamine metabolism in health and disease. *Biochimica et Biophysica Acta (BBA) - Biomembranes* **2017**, *1859*, 1558-1572, doi:https://doi.org/10.1016/j.bbamem.2017.04.006.
20. Skotland, T.; Kavaliauskiene, S.; Sandvig, K. The role of lipid species in membranes and cancer-related changes. *Cancer and Metastasis Reviews* **2020**, *39*, 343-360, doi:10.1007/s10555-020-09872-z.
21. Hörl, G.; Wagner, A.; Cole, L.K.; Malli, R.; Reicher, H.; Kotzbeck, P.; Köfeler, H.; Höfler, G.; Frank, S.; Bogner-Strauss, J.G.; et al. Sequential synthesis and methylation of phosphatidylethanolamine promote lipid droplet biosynthesis and stability in tissue culture and in vivo. *J Biol Chem* **2011**, *286*, 17338-17350, doi:10.1074/jbc.M111.234534.
22. Saito, R.d.F.; Andrade, L.N.d.S.; Bustos, S.O.; Chammas, R. Phosphatidylcholine-Derived Lipid Mediators: The Crosstalk Between Cancer Cells and Immune Cells. *Frontiers in Immunology* **2022**, *13*, doi:10.3389/fimmu.2022.768606.
23. van der Veen, J.N.; Lingrell, S.; McCloskey, N.; LeBlond, N.D.; Galleguillos, D.; Zhao, Y.Y.; Curtis, J.M.; Sipione, S.; Fullerton, M.D.; Vance, D.E.; et al. A role for phosphatidylcholine and phosphatidylethanolamine in hepatic insulin signaling. *FASEB J* **2019**, *33*, 5045-5057, doi:10.1096/fj.201802117R.
24. Vance, D.E. Physiological roles of phosphatidylethanolamine N-methyltransferase. *Biochimica et Biophysica Acta (BBA) - Molecular and Cell Biology of Lipids* **2013**, *1831*, 626-632, doi:https://doi.org/10.1016/j.bbalip.2012.07.017.

25. Keogh, M.R.; Courtney, P.D.; Kinney, A.J.; Dewey, R.E. Functional characterization of phospholipid N-methyltransferases from Arabidopsis and soybean. *The Journal of biological chemistry* **2009**, *284*, 15439-15447, doi:10.1074/jbc.M109.005991.
26. Gaynor, P.M.; Carman, G.M. Phosphatidylethanolamine methyltransferase and phospholipid methyltransferase activities from Saccharomyces cerevisiae. Enzymological and kinetic properties. *Biochim Biophys Acta* **1990**, *1045*, 156-163, doi:10.1016/0005-2760(90)90145-n.
27. Moessinger, C.; Klizaite, K.; Steinhagen, A.; Philippou-Massier, J.; Shevchenko, A.; Hoch, M.; Ejsing, C.S.; Thiele, C. Two different pathways of phosphatidylcholine synthesis, the Kennedy Pathway and the Lands Cycle, differentially regulate cellular triacylglycerol storage. *BMC Cell Biology* **2014**, *15*, 43, doi:10.1186/s12860-014-0043-3.
28. Reo, N.V.; Adinehzadeh, M.; Foy, B.D. Kinetic analyses of liver phosphatidylcholine and phosphatidylethanolamine biosynthesis using 13C NMR spectroscopy. *Biochimica et Biophysica Acta (BBA) - Molecular and Cell Biology of Lipids* **2002**, *1580*, 171-188, doi:https://doi.org/10.1016/S1388-1981(01)00202-5.
29. Cui, Z.; Vance, J.E.; Chen, M.H.; Voelker, D.R.; Vance, D.E. Cloning and expression of a novel phosphatidylethanolamine N-methyltransferase. A specific biochemical and cytological marker for a unique membrane fraction in rat liver. *Journal of Biological Chemistry* **1993**, *268*, 16655-16663, doi:https://doi.org/10.1016/S0021-9258(19)85468-6.
30. Vance, D.E.; Walkey, C.J.; Cui, Z. Phosphatidylethanolamine N-methyltransferase from liver. *Biochimica et Biophysica Acta (BBA) - Lipids and Lipid Metabolism* **1997**, *1348*, 142-150, doi:https://doi.org/10.1016/S0005-2760(97)00108-2.
31. Walkey, C.J.; Donohue, L.R.; Bronson, R.; Agellon, L.B.; Vance, D.E. Disruption of the murine gene encoding phosphatidylethanolamine N-methyltransferase. *Proc Natl Acad Sci U S A* **1997**, *94*, 12880-12885, doi:10.1073/pnas.94.24.12880.
32. Gibellini, F.; Smith, T.K. The Kennedy pathway—De novo synthesis of phosphatidylethanolamine and phosphatidylcholine. *IUBMB Life* **2010**, *62*, 414-428, doi:https://doi.org/10.1002/iub.337.
33. Noga, A.A.; Zhao, Y.; Vance, D.E. An Unexpected Requirement for PhosphatidylethanolamineN-Methyltransferase in the Secretion of Very Low Density Lipoproteins *. *Journal of Biological Chemistry* **2002**, *277*, 42358-42365, doi:10.1074/jbc.M204542200.
34. Zhao, Y.; Su, B.; Jacobs, R.L.; Kennedy, B.; Francis, G.A.; Waddington, E.; Brosnan, J.T.; Vance, J.E.; Vance, D.E. Lack of phosphatidylethanolamine N-methyltransferase alters plasma VLDL phospholipids and attenuates atherosclerosis in mice. *Arterioscler Thromb Vasc Biol* **2009**, *29*, 1349-1355, doi:10.1161/atvbaha.109.188672.
35. DeLong, C.J.; Shen, Y.-J.; Thomas, M.J.; Cui, Z. Molecular Distinction of Phosphatidylcholine Synthesis between the CDP-Choline Pathway and Phosphatidylethanolamine Methylation Pathway*. *Journal of Biological Chemistry* **1999**, *274*, 29683-29688, doi:https://doi.org/10.1074/jbc.274.42.29683.
36. Boumann, H.A.; Damen, M.J.A.; Versluis, C.; Heck, A.J.R.; de Kruijff, B.; de Kroon, A.I.P.M. The Two Biosynthetic Routes Leading to Phosphatidylcholine in Yeast Produce Different Sets of Molecular Species. Evidence for Lipid Remodeling. *Biochemistry* **2003**, *42*, 3054-3059, doi:10.1021/bi026801r.
37. Watkins, S.M.; Zhu, X.; Zeisel, S.H. Phosphatidylethanolamine-N-methyltransferase Activity and Dietary Choline Regulate Liver-Plasma Lipid Flux and Essential Fatty Acid Metabolism in Mice. *The Journal of Nutrition* **2003**, *133*, 3386-3391, doi:10.1093/jn/133.11.3386.
38. van der Veen, J.N.; Lingrell, S.; da Silva, R.P.; Jacobs, R.L.; Vance, D.E. The Concentration of Phosphatidylethanolamine in Mitochondria Can Modulate ATP Production and Glucose Metabolism in Mice. *Diabetes* **2014**, *63*, 2620-2630, doi:10.2337/db13-0993.
39. Zhu, X.; Song, J.; Mar, M.-H.; Edwards, L.J.; Zeisel, S.H. Phosphatidylethanolamine N-methyltransferase (PEMT) knockout mice have hepatic steatosis and abnormal hepatic choline metabolite concentrations despite ingesting a recommended dietary intake of choline. *Biochem J* **2003**, *370*, 987-993, doi:10.1042/BJ20021523.

40. Watanabe, M.; Nakatsuka, A.; Murakami, K.; Inoue, K.; Terami, T.; Higuchi, C.; Katayama, A.; Teshigawara, S.; Eguchi, J.; Ogawa, D.; et al. Pemt deficiency ameliorates endoplasmic reticulum stress in diabetic nephropathy. *PloS one* **2014**, *9*, e92647-e92647, doi:10.1371/journal.pone.0092647.
41. Nakatsuka, A.; Matsuyama, M.; Yamaguchi, S.; Katayama, A.; Eguchi, J.; Murakami, K.; Teshigawara, S.; Ogawa, D.; Wada, N.; Yasunaka, T.; et al. Insufficiency of phosphatidylethanolamine N-methyltransferase is risk for lean non-alcoholic steatohepatitis. *Scientific Reports* **2016**, *6*, 21721, doi:10.1038/srep21721.
42. Gao, X.; van der Veen, J.N.; Fernandez-Patron, C.; Vance, J.E.; Vance, D.E.; Jacobs, R.L. Insufficient glucose supply is linked to hypothermia upon cold exposure in high-fat diet-fed mice lacking PEMT [S]. *Journal of Lipid Research* **2015**, *56*, 1701-1710, doi:10.1194/jlr.M059287.
43. Jacobs, R.L.; Zhao, Y.; Koonen, D.P.; Sletten, T.; Su, B.; Lingrell, S.; Cao, G.; Peake, D.A.; Kuo, M.S.; Proctor, S.D.; et al. Impaired de novo choline synthesis explains why phosphatidylethanolamine N-methyltransferase-deficient mice are protected from diet-induced obesity. *J Biol Chem* **2010**, *285*, 22403-22413, doi:10.1074/jbc.M110.108514.
44. Sun, X.; Chen, W.-D.; Wang, Y.-D. DAF-16/FOXO Transcription Factor in Aging and Longevity. *Frontiers in Pharmacology* **2017**, *8*, doi:10.3389/fphar.2017.00548.
45. Park, S.; Kim, B.-K.; Park, S.-K. Supplementation with phosphatidylethanolamine confers anti-oxidant and anti-aging effects via hormesis and reduced insulin/IGF-1-like signaling in C. elegans. *Mechanisms of Ageing and Development* **2021**, *197*, 111498, doi:https://doi.org/10.1016/j.mad.2021.111498.
46. Kim, S.H.; Kim, B.K.; Park, S.; Park, S.K. Phosphatidylcholine Extends Lifespan via DAF-16 and Reduces Amyloid-Beta-Induced Toxicity in Caenorhabditis elegans. *Oxid Med Cell Longev* **2019**, *2019*, 2860642, doi:10.1155/2019/2860642.
47. Gao, A.W.; Chatzispyrou, I.A.; Kamble, R.; Liu, Y.J.; Herzog, K.; Smith, R.L.; van Lenthe, H.; Vervaart, M.A.T.; van Cruchten, A.; Luyf, A.C.; et al. A sensitive mass spectrometry platform identifies metabolic changes of life history traits in C. elegans. *Scientific Reports* **2017**, *7*, 2408, doi:10.1038/s41598-017-02539-w.
48. Braun, F.; Rinschen, M.M.; Bartels, V.; Frommolt, P.; Habermann, B.; Hoeijmakers, J.H.J.; Schumacher, B.; Dollé, M.E.T.; Müller, R.-U.; Benzing, T.; et al. Altered lipid metabolism in the aging kidney identified by three layered omic analysis. *Aging* **2016**, *8*, 441-454, doi:10.18632/aging.100900.
49. Rockenfeller, P.; Koska, M.; Pietrocola, F.; Minois, N.; Knittelfelder, O.; Sica, V.; Franz, J.; Carmona-Gutierrez, D.; Kroemer, G.; Madeo, F. Phosphatidylethanolamine positively regulates autophagy and longevity. *Cell Death & Differentiation* **2015**, *22*, 499-508, doi:10.1038/cdd.2014.219.
50. Kõks, S.; Dogan, S.; Tuna, B.G.; González-Navarro, H.; Potter, P.; Vandenbroucke, R.E. Mouse models of ageing and their relevance to disease. *Mechanisms of Ageing and Development* **2016**, *160*, 41-53, doi:https://doi.org/10.1016/j.mad.2016.10.001.
51. Vandamme, T.F. Use of rodents as models of human diseases. *J Pharm Bioallied Sci* **2014**, *6*, 2-9, doi:10.4103/0975-7406.124301.
52. Zhou, Q.; Kerbl-Knapp, J.; Zhang, F.; Korbelius, M.; Kuentzel, K.B.; Vujić, N.; Akhmetshina, A.; Hörl, G.; Paar, M.; Steyrer, E.; et al. Metabolomic Profiles of Mouse Tissues Reveal an Interplay between Aging and Energy Metabolism. *Metabolites* **2022**, *12*, doi:10.3390/metabo12010017.
53. Vance, D.E. Phospholipid methylation in mammals: from biochemistry to physiological function. *Biochimica et Biophysica Acta (BBA) - Biomembranes* **2014**, *1838*, 1477-1487, doi:https://doi.org/10.1016/j.bbamem.2013.10.018.
54. Loria, J.P.; Rance, M.; Palmer, A.G. A Relaxation-Compensated Carr−Purcell−Meiboom−Gill Sequence for Characterizing Chemical Exchange by NMR Spectroscopy. *Journal of the American Chemical Society* **1999**, *121*, 2331-2332, doi:10.1021/ja983961a.
55. Vignoli, A.; Ghini, V.; Meoni, G.; Licari, C.; Takis, P.G.; Tenori, L.; Turano, P.; Luchinat, C. High-Throughput Metabolomics by 1D NMR. *Angew Chem Int Ed Engl* **2019**, *58*, 968-994, doi:10.1002/anie.201804736.

56. Stryeck, S.; Gastrager, M.; Degoricija, V.; Trbušić, M.; Potočnjak, I.; Radulović, B.; Pregartner, G.; Berghold, A.; Madl, T.; Frank, S. Serum Concentrations of Citrate, Tyrosine, 2- and 3- Hydroxybutyrate are Associated with Increased 3-Month Mortality in Acute Heart Failure Patients. *Sci Rep* **2019**, *9*, 6743, doi:10.1038/s41598-019-42937-w.
57. Xia, J.; Wishart, D.S. MSEA: a web-based tool to identify biologically meaningful patterns in quantitative metabolomic data. *Nucleic Acids Res* **2010**, *38*, W71-77, doi:10.1093/nar/gkq329.
58. Pang, Z.; Chong, J.; Zhou, G.; de Lima Morais, D.A.; Chang, L.; Barrette, M.; Gauthier, C.; Jacques, P.-É.; Li, S.; Xia, J. MetaboAnalyst 5.0: narrowing the gap between raw spectra and functional insights. *Nucleic Acids Research* **2021**, *49*, W388-W396, doi:10.1093/nar/gkab382.
59. Zhang, F.; Kerbl-Knapp, J.; Akhmetshina, A.; Korbelius, M.; Kuentzel, K.B.; Vujić, N.; Hörl, G.; Paar, M.; Kratky, D.; Steyrer, E.; et al. Tissue-Specific Landscape of Metabolic Dysregulation during Ageing. *Biomolecules* **2021**, *11*, doi:10.3390/biom11020235.
60. Verkerke, A.R.P.; Ferrara, P.J.; Lin, C.-T.; Johnson, J.M.; Ryan, T.E.; Maschek, J.A.; Eshima, H.; Paran, C.W.; Laing, B.T.; Siripoksup, P.; et al. Phospholipid methylation regulates muscle metabolic rate through Ca(2+) transport efficiency. *Nat Metab* **2019**, *1*, 876-885, doi:10.1038/s42255-019-0111-2.
61. Johnson, J.M.; Verkerke, A.R.P.; Maschek, J.A.; Ferrara, P.J.; Lin, C.-T.; Kew, K.A.; Neufer, P.D.; Lodhi, I.J.; Cox, J.E.; Funai, K. Alternative splicing of UCP1 by non-cell-autonomous action of PEMT. *Molecular Metabolism* **2020**, *31*, 55-66, doi:https://doi.org/10.1016/j.molmet.2019.10.007.
62. Yao, Z.M.; Vance, D.E. The active synthesis of phosphatidylcholine is required for very low density lipoprotein secretion from rat hepatocytes. *J Biol Chem* **1988**, *263*, 2998-3004.
63. Yao, Z.M.; Vance, D.E. Head Group Specificity in the Requirement of Phosphatidylcholine Biosynthesis for Very Low Density Lipoprotein Secretion from Cultured Hepatocytes. *Journal of Biological Chemistry* **1989**, *264*, 11373-11380, doi:https://doi.org/10.1016/S0021-9258(18)60474-0.
64. Song, J.; da Costa, K.A.; Fischer, L.M.; Kohlmeier, M.; Kwock, L.; Wang, S.; Zeisel, S.H. Polymorphism of the PEMT gene and susceptibility to nonalcoholic fatty liver disease (NAFLD). *FASEB J* **2005**, *19*, 1266-1271, doi:10.1096/fj.04-3580com.
65. Fagone, P.; Jackowski, S. Phosphatidylcholine and the CDP-choline cycle. *Biochim Biophys Acta* **2013**, *1831*, 523-532, doi:10.1016/j.bbalip.2012.09.009.
66. Serviddio, G.; Bellanti, F.; Tamborra, R.; Rollo, T.; Capitanio, N.; Romano, A.D.; Sastre, J.; Vendemiale, G.; Altomare, E. Uncoupling protein-2 (UCP2) induces mitochondrial proton leak and increases susceptibility of non-alcoholic steatohepatitis (NASH) liver to ischaemia–reperfusion injury. *Gut* **2008**, *57*, 957, doi:10.1136/gut.2007.147496.
67. Al Rajabi, A.; Castro, G.S.F.; da Silva, R.P.; Nelson, R.C.; Thiesen, A.; Vannucchi, H.; Vine, D.F.; Proctor, S.D.; Field, C.J.; Curtis, J.M.; et al. Choline Supplementation Protects against Liver Damage by Normalizing Cholesterol Metabolism in Pemt/Ldlr Knockout Mice Fed a High-Fat Diet. *The Journal of Nutrition* **2014**, *144*, 252-257, doi:10.3945/jn.113.185389.
68. Lu, S.C. Dysregulation of glutathione synthesis in liver disease. *Liver Research* **2020**, *4*, 64-73, doi:https://doi.org/10.1016/j.livres.2020.05.003.
69. Brosnan, M.E.; Brosnan, J.T. Histidine Metabolism and Function. *J Nutr* **2020**, *150*, 2570s-2575s, doi:10.1093/jn/nxaa079.
70. Cruzat, V.; Macedo Rogero, M.; Noel Keane, K.; Curi, R.; Newsholme, P. Glutamine: Metabolism and Immune Function, Supplementation and Clinical Translation. *Nutrients* **2018**, *10*, doi:10.3390/nu10111564.
71. Martínez-Reyes, I.; Chandel, N.S. Mitochondrial TCA cycle metabolites control physiology and disease. *Nature Communications* **2020**, *11*, 102, doi:10.1038/s41467-019-13668-3.
72. Fushimi, T.; Tayama, K.; Fukaya, M.; Kitakoshi, K.; Nakai, N.; Tsukamoto, Y.; Sato, Y. Acetic acid feeding enhances glycogen repletion in liver and skeletal muscle of rats. *J Nutr* **2001**, *131*, 1973-1977, doi:10.1093/jn/131.7.1973.

73. Staels, B.; Fonseca, V.A. Bile acids and metabolic regulation: mechanisms and clinical responses to bile acid sequestration. *Diabetes Care* **2009**, *32 Suppl 2*, S237-245, doi:10.2337/dc09-S355.
74. Lawton, K.A.; Berger, A.; Mitchell, M.; Milgram, K.E.; Evans, A.M.; Guo, L.; Hanson, R.W.; Kalhan, S.C.; Ryals, J.A.; Milburn, M.V. Analysis of the adult human plasma metabolome. *Pharmacogenomics* **2008**, *9*, 383-397, doi:10.2217/14622416.9.4.383.
75. Li, J.; Guasch-Ferré, M.; Chung, W.; Ruiz-Canela, M.; Toledo, E.; Corella, D.; Bhupathiraju, S.N.; Tobias, D.K.; Tabung, F.K.; Hu, J.; et al. The Mediterranean diet, plasma metabolome, and cardiovascular disease risk. *European Heart Journal* **2020**, *41*, 2645-2656, doi:10.1093/eurheartj/ehaa209.
76. Banoglu, E.; Jha, G.G.; King, R.S. Hepatic microsomal metabolism of indole to indoxyl, a precursor of indoxyl sulfate. *European Journal of Drug Metabolism and Pharmacokinetics* **2001**, *26*, 235-240, doi:10.1007/BF03226377.
77. Leong, S.C.; Sirich, T.L. Indoxyl Sulfate—Review of Toxicity and Therapeutic Strategies. *Toxins* **2016**, *8*, doi:10.3390/toxins8120358.
78. Stryeck, S.; Birner-Gruenberger, R.; Madl, T. Integrative metabolomics as emerging tool to study autophagy regulation. *Microb Cell* **2017**, *4*, 240-258, doi:10.15698/mic2017.08.584.
79. Antonsson, B. Phosphatidylinositol synthase from mammalian tissues1Dedicated to Professor Eugene Kennedy.1. *Biochimica et Biophysica Acta (BBA) - Lipids and Lipid Metabolism* **1997**, *1348*, 179-186, doi:https://doi.org/10.1016/S0005-2760(97)00105-7.
80. Wan, S.; van der Veen, J.N.; N'Goma, J.-C.B.; Nelson, R.C.; Vance, D.E.; Jacobs, R.L. Hepatic PEMT activity mediates liver health, weight gain, and insulin resistance. *The FASEB Journal* **2019**, *33*, 10986-10995, doi:https://doi.org/10.1096/fj.201900679R.
81. Duncan, R.E.; Ahmadian, M.; Jaworski, K.; Sarkadi-Nagy, E.; Sul, H.S. Regulation of Lipolysis in Adipocytes. *Annual Review of Nutrition* **2007**, *27*, 79-101, doi:10.1146/annurev.nutr.27.061406.093734.
82. Tanaka, T.; Mochida, T.; Maki, Y.; Shiraki, Y.; Mori, H.; Matsumoto, S.; Shimbo, K.; Ando, T.; Nakamura, K.; Endo, F.; et al. Interactive network analysis of the plasma amino acids profile in a mouse model of hyperglycemia. *Springerplus* **2013**, *2*, 287-287, doi:10.1186/2193-1801-2-287.
83. Zampino, M.; AlGhatrif, M.; Kuo, P.-L.; Simonsick, E.M.; Ferrucci, L. Longitudinal Changes in Resting Metabolic Rates with Aging Are Accelerated by Diseases. *Nutrients* **2020**, *12*, 3061, doi:10.3390/nu12103061.
84. Tretter, L.; Patocs, A.; Chinopoulos, C. Succinate, an intermediate in metabolism, signal transduction, ROS, hypoxia, and tumorigenesis. *Biochimica et Biophysica Acta (BBA) - Bioenergetics* **2016**, *1857*, 1086-1101, doi:https://doi.org/10.1016/j.bbabio.2016.03.012.
85. Walkey, C.J.; Donohue, L.R.; Bronson, R.; Agellon, L.B.; Vance, D.E. Disruption of the murine gene encoding phosphatidylethanolamine N-methyltransferase. *Proceedings of the National Academy of Sciences* **1997**, *94*, 12880-12885, doi:doi:10.1073/pnas.94.24.12880.
86. Li, Z.; Vance, D.E. Thematic Review Series: Glycerolipids. Phosphatidylcholine and choline homeostasis. *Journal of Lipid Research* **2008**, *49*, 1187-1194, doi:https://doi.org/10.1194/jlr.R700019-JLR200.
87. Shiao, Y.J.; Vance, J.E. Evidence for an ethanolamine cycle: differential recycling of the ethanolamine moiety of phosphatidylethanolamine derived from phosphatidylserine and ethanolamine. *Biochem J* **1995**, *310 (Pt 2)*, 673-679, doi:10.1042/bj3100673.
88. Fernández-Murray, J.P.; McMaster, C.R. Glycerophosphocholine Catabolism as a New Route for Choline Formation for Phosphatidylcholine Synthesis by the Kennedy Pathway*. *Journal of Biological Chemistry* **2005**, *280*, 38290-38296, doi:https://doi.org/10.1074/jbc.M507700200.
89. Morash, S.C.; Cook, H.W.; Spence, M.W. Phosphatidylcholine metabolism in cultured cells: catabolism via glycerophosphocholine. *Biochim Biophys Acta* **1988**, *961*, 194-202, doi:10.1016/0005-2760(88)90114-2.

90. Sonkar, K.; Ayyappan, V.; Tressler, C.M.; Adelaja, O.; Cai, R.; Cheng, M.; Glunde, K. Focus on the glycerophosphocholine pathway in choline phospholipid metabolism of cancer. *NMR Biomed* **2019**, *32*, e4112-e4112, doi:10.1002/nbm.4112.
91. Shinde, A.B.; Song, A.; Wang, Q.A. Brown Adipose Tissue Heterogeneity, Energy Metabolism, and Beyond. *Front Endocrinol (Lausanne)* **2021**, *12*, doi:10.3389/fendo.2021.651763.
92. Maltais-Payette, I.; Boulet, M.-M.; Prehn, C.; Adamski, J.; Tchernof, A. Circulating glutamate concentration as a biomarker of visceral obesity and associated metabolic alterations. *Nutrition & Metabolism* **2018**, *15*, 78, doi:10.1186/s12986-018-0316-5.
93. Sun, W.; Dong, H.; Wolfrum, C. Local acetate inhibits brown adipose tissue function. *Proceedings of the National Academy of Sciences* **2021**, *118*, e2116125118, doi:10.1073/pnas.2116125118.
94. Santos, G.M.; Neves, F.d.A.R.; Amato, A.A. Thermogenesis in white adipose tissue: An unfinished story about PPARγ. *Biochimica et Biophysica Acta (BBA) - General Subjects* **2015**, *1850*, 691-695, doi:https://doi.org/10.1016/j.bbagen.2015.01.002.
95. Trayhurn, P.; Beattie, J.H. Physiological role of adipose tissue: white adipose tissue as an endocrine and secretory organ. *Proc Nutr Soc* **2001**, *60*, 329-339, doi:10.1079/pns200194.
96. Gao, X.; van der Veen, J.N.; Hermansson, M.; Ordoñez, M.; Gomez-Muñoz, A.; Vance, D.E.; Jacobs, R.L. Decreased lipogenesis in white adipose tissue contributes to the resistance to high fat diet-induced obesity in phosphatidylethanolamine N-methyltransferase-deficient mice. *Biochimica et Biophysica Acta (BBA) - Molecular and Cell Biology of Lipids* **2015**, *1851*, 152-162, doi:https://doi.org/10.1016/j.bbalip.2014.11.006.
97. Amelio, I.; Cutruzzolá, F.; Antonov, A.; Agostini, M.; Melino, G. Serine and glycine metabolism in cancer. *Trends Biochem Sci* **2014**, *39*, 191-198, doi:10.1016/j.tibs.2014.02.004.
98. Krivoruchko, A.; Zhang, Y.; Siewers, V.; Chen, Y.; Nielsen, J. Microbial acetyl-CoA metabolism and metabolic engineering. *Metabolic Engineering* **2015**, *28*, 28-42, doi:https://doi.org/10.1016/j.ymben.2014.11.009.
99. Voshol, P.J.; Minich, D.M.; Havinga, R.; Elferink, R.P.J.O.; Verkade, H.J.; Groen, A.K.; Kuipers, F. Postprandial chylomicron formation and fat absorption in multidrug resistance gene 2 P-glycoprotein–deficient mice. *Gastroenterology* **2000**, *118*, 173-182, doi:https://doi.org/10.1016/S0016-5085(00)70426-4.
100. Verkade, H.J.; Havinga, R.; Shields, D.J.; Wolters, H.; Bloks, V.W.; Kuipers, F.; Vance, D.E.; Agellon, L.B. The phosphatidylethanolamine N-methyltransferase pathway is quantitatively not essential for biliary phosphatidylcholine secretion. *Journal of Lipid Research* **2007**, *48*, 2058-2064, doi:https://doi.org/10.1194/jlr.M700278-JLR200.
101. Li, Z.; Agellon, L.B.; Vance, D.E. The role of phosphatidylethanolamine methyltransferase in a mouse model of intrahepatic cholestasis. *Biochimica et Biophysica Acta (BBA) - Molecular and Cell Biology of Lipids* **2011**, *1811*, 278-283, doi:https://doi.org/10.1016/j.bbalip.2011.01.006.
102. Parthasarathy, S.; Subbaiah, P.V.; Ganguly, J. The mechanism of intestinal absorption of phosphatidylcholine in rats. *Biochem J* **1974**, *140*, 503-508, doi:10.1042/bj1400503.
103. Luise, D.; Correa, F.; Bosi, P.; Trevisi, P. A Review of the Effect of Formic Acid and Its Salts on the Gastrointestinal Microbiota and Performance of Pigs. *Animals (Basel)* **2020**, *10*, 887, doi:10.3390/ani10050887.
104. Pietzke, M.; Meiser, J.; Vazquez, A. Formate metabolism in health and disease. *Molecular Metabolism* **2020**, *33*, 23-37, doi:https://doi.org/10.1016/j.molmet.2019.05.012.
105. Zhou, J.; Xiong, X.; Wang, K.X.; Zou, L.J.; Ji, P.; Yin, Y.L. Ethanolamine enhances intestinal functions by altering gut microbiome and mucosal anti-stress capacity in weaned rats. *Br J Nutr* **2018**, *120*, 241-249, doi:10.1017/s0007114518001101.
106. Faelli, A.; Esposito, G. Effect of inosine and its metabolites on intestinal iron absorption in the rat. *Biochemical Pharmacology* **1970**, *19*, 2551-2554, doi:https://doi.org/10.1016/0006-2952(70)90003-1.